High order conservative finite difference WENO scheme for three-temperature radiation hydrodynamics

Juan Cheng[1] and Chi-Wang Shu[2]

Abstract

The three-temperature (3-T) radiation hydrodynamics (RH) equations play an important role in the high-energy-density-physics fields, such as astrophysics and inertial confinement fusion (ICF). It describes the interaction between radiation and high-energy-density plasmas including electron and ion in the assumption that radiation, electron and ion are in their own equilibrium state, which means they can be characterized by their own temperature. The 3-T RH system consists of the density, momentum and three internal energy (electron, ion and radiation) equations. In this paper, we propose a high order conservative finite difference weighted essentially non-oscillatory (WENO) scheme solving one-dimensional (1D) and two-dimensional (2D) 3-T RH equations respectively. Following our previous paper [7], we introduce the three new energy variables, and then design a finite difference scheme with both conservative property and arbitrary high order accuracy. Based on the WENO interpolation and the strong stability preserving (SSP) high order time discretizations, taken as an example, we design a class of fifth order conservative finite difference schemes in space and third order in time. Compared with the Lagrangian method we proposed in [7], which can only reach second order accuracy for 2D 3-T RH equations if straight-line edged meshes are used, the finite difference scheme can be easily designed to arbitrary high order accuracy for multi-dimensional 3-T RH equations. The finite difference formulation is also much less expensive in multi-dimensions than finite volume schemes used in [7]. Furthermore, our method can handle fluids with large deformation easily. Numerous 1D and 2D numerical examples are presented to verify the desired properties of the high order finite difference WENO schemes such as high order accuracy, non-oscillation, conservation and adaptation to severely distorted single-material radiation hydrodynamics problems.

Keywords: finite difference method; high order; conservative; WENO, radiation hydrodynamics equations; three-temperature

AMS subject classification: 65M06

[1]Corresponding author. Laboratory of Computational Physics, Institute of Applied Physics and Computational Mathematics, Beijing 100088, China and HEDPS, Center for Applied Physics and Technology, and College of Engineering, Peking University, Beijing 100871, China. E-mail: cheng_juan@iapcm.ac.cn. Research is supported in part by NSFC grant 12031001 and National Key R&D Program of China No. 2022YFA1004500.

[2]Division of Applied Mathematics, Brown University, Providence, RI 02912, USA. E-mail: chi-wang_shu@brown.edu. Research is supported in part by NSF grant DMS-2309249.

1 Introduction

The three-temperature (3-T) radiation hydrodynamics (RH) equations are used to describe the interaction between radiation and high-energy-density plasmas including electron and ion in the assumption that each of electron, ion and radiation is in its own equilibrium state, which means they can be characterized by their own temperatures, and these three temperatures are usually not equal. The 3-T RH equations are widely used in depicting the optically thick high-energy-density-physics problems such as those in astrophysics and inertial confinement fusion (ICF) [2, 9, 13].

In this paper, we continue our study in [7] on high order numerical methods for solving the 3-T RH equations. The 3-T RH equations consist of five equations (in 1D), namely those for density, momentum, and three internal energies (electron, ion and radiation). However there are only three conservation laws, namely those for mass, momentum and total energy. The total energy, namely the sum of the three internal energies and the kinetic energy, is conserved. As the three internal energy equations contain the non-conservative terms, when summing up the three internal energies and the kinetic energy, we should get a conservative scheme for the total energy, but this is very difficult to achieve because the kinetic energy is a nonlinear function of the two conserved quantities, i.e., density and momentum. Previous efforts [1, 14, 3] would try to combine the schemes for the internal energies and for the density and momentum in a nonlinear way, also at different time levels, in order to achieve conservation for the total energy. This procedure is difficult for achieving high order accuracy, especially high order accuracy in time.

In [7], we introduced three new energy variables by adding a third of the kinetic energy to each of the corresponding internal energies. The 3-T RH equations are rewritten in the form of the three new energy equations. The advantage of doing this is that, although each of the three energy equations for the three new energy variables still contain non-conservative terms, the sum of these three energy equations is automatically the conservation law for the total energy. Therefore, as long as the numerical approximations to the non-conservative terms in the three energy equations are designed such that they sum to zero over all three energy equations, we automatically obtain a conservative scheme for the total energy.

There are some literatures on the numerical methods for the 3-T RH equations. In [6], by the establishment of an equivalency relationship between the discretizations of the total energy equation and the internal energy equation, the authors developed a cell-centered first order Lagrangian scheme for the 3-T RH equations which can keep the conservation of mass, momentum and total energy. In [17, 18], a 3-T RH code based on the Lagrangian method was developed in two-dimensional (2D) axis-symmetric geometries. In [3], a first order

positivity-preserving, conservative and entropy-stable Lagrangian scheme was presented for the 3-T RH equations. In [10], the numerical comparisons among three famous simulation codes (FLASH, RAGE and CRASH) solving the 3-T RH system were given. More recently, in [7], the authors constructed a class of high order conservative Lagrangian schemes for one and two dimensional 3-T RH equations based on the multi-resolution WENO reconstruction and the strong stability preserving (SSP) high order time discretizations. By introducing three new energy variables, the three energy equations in the 3-T RH system are rewritten in the new form, based on which the schemes can be designed to keep the conservation of mass, momentum and total energy.

Most of the above mentioned existing numerical methods solving the 3-T RH equations are designed based on the Lagrangian formulation. The Lagrangian schemes are good especially for multi-material flows, but they are prone to suffer from lack of robustness because of the mesh distortion and the need of remapping when the mesh quality becomes poor. In particular, for the problems with physical slip line instabilities such as Rayleigh-Taylor (RT) and Richtmyer-Meshkov (RM) instabilities, it is almost impossible to keep the slip line intact as a mesh line, hence the Eulerian methods would be preferred to solve these kinds of problems.

In this paper, we propose a high order finite difference Eulerian scheme for the 3-T RH equations with the Cartesian meshes on the regular geometry. In such situation the finite difference scheme is much more efficient than the finite volume scheme [15]. We study the fifth order finite difference weighted essentially non-oscillatory (WENO) scheme as an example, which is suitable for the single material 3-T RH problems. The WENO scheme is high order accurate scheme designed for problems with piecewise smooth solutions containing discontinuities. The key idea lies at the approximation level, where nonlinear weights are designed to automatically choose more information from the locally smoother stencil, hence reducing the artifacts from crossing discontinuities in the approximation procedure as much as possible. For more details we refer to [12, 15]. To achieve high order accuracy in time, the SSP high order time discretizations is adopted.

An outline of the rest of this paper is as follows. In Section 2, taking the 2D three temperature radiation hydrodynamics equations as an example, we will introduce the Jacobian matrices, eigenvalues and eigenvectors corresponding to the convection terms of the equations, which will be used in local characteristic decomposition for high order schemes. In Section 3, we will propose a fifth order explicit conservative finite difference scheme solving the 1D 3-T RH equations. In Section 4, we will describe a fifth order explicit conservative finite difference scheme solving the 2D 3-T RH equations. In Section 5, various 1D and 2D numerical examples will be given to demonstrate the good performance of the new fi-

nite difference WENO schemes including high order accuracy, non-oscillation, conservation and adaptation to severely distorted single-material radiation hydrodynamics problems. In Section 6, we will give concluding remarks.

2 Three temperature radiation hydrodynamics equations

We consider the three-temperature radiation hydrodynamics equations, which have the following form in two dimensional Cartesian coordinates,

$$
\begin{cases}
\partial_t \rho + \nabla \cdot (\rho \mathbf{w}) = 0 \\
\partial_t \rho u + \nabla \cdot (\rho u \mathbf{w}) + \partial_x p = 0 \\
\partial_t \rho v + \nabla \cdot (\rho v \mathbf{w}) + \partial_y p = 0 \\
\partial_t \rho e_e + \nabla \cdot (\rho e_e \mathbf{w}) + p_e \nabla \cdot \mathbf{w} = \nabla \cdot (\kappa_e \nabla T_e) - \omega_{ei}(T_e - T_i) - \omega_{er}(T_e^4 - T_r^4) \\
\partial_t \rho e_i + \nabla \cdot (\rho e_i \mathbf{w}) + p_i \nabla \cdot \mathbf{w} = \nabla \cdot (\kappa_i \nabla T_i) + \omega_{ei}(T_e - T_i) \\
\partial_t \rho e_r + \nabla \cdot (\rho e_r \mathbf{w}) + p_r \nabla \cdot \mathbf{w} = \nabla \cdot (\kappa_r \nabla T_r) + \omega_{er}(T_e^4 - T_r^4)
\end{cases}
\tag{2.1}
$$

where ρ is the density, $\mathbf{w} = (u, v)$ is the velocity. $\{e_e, e_i, e_r\}$, $\{p_e, p_i, p_r\}$, $\{T_e, T_i, T_r\}$ and $\{\kappa_e, \kappa_i, \kappa_r\}$ are the specific internal energy, pressure, temperature and conduction coefficients for electron, ion and radiation respectively. $p = p_e + p_i + p_r$ is the total pressure. ω_{ei} is the energy-exchange coefficient between electron and ion, ω_{er} is the energy-exchange coefficient between electron and radiation. $\nabla = (\partial_x, \partial_y)$ is the divergence operator. The system (2.1) represents the conservation of mass, momentum in the x and y directions and total energy, where the total energy is $E = \rho(e_e + e_i + e_r) + \frac{1}{2}\rho(u^2 + v^2)$. The relationship between the three specific internal energies and temperatures is as follows,

$$
e_e = c_{ve} T_e, \quad e_i = c_{vi} T_i, \quad e_r = a T_r^4 / \rho,
$$

where c_{ve} and c_{vi} are the heat capacity at constant volume of electron and ion respectively, and a is the radiation constant.

The set of equations need to be completed by the addition of the matter's equations of state (EOS) with the following general form,

$$
p_e = p(\rho, e_e), \quad p_i = p(\rho, e_i).
\tag{2.2}
$$

Especially, if we consider the γ-law gas, then the equations of state (EOS) have the following simpler form,

$$
p_e = (\gamma_e - 1)\rho e_e, \quad p_i = (\gamma_i - 1)\rho e_i,
\tag{2.3}
$$

where γ_e, γ_i are the constants representing the ratio of specific heat capacities of the electron and ion respectively. Also $p_r = \frac{1}{3}\rho e_r$, and we can rewrite p_r in the similar form as p_e, p_i in

(2.3), that is,

$$p_r = (\gamma_r - 1)\rho e_r \tag{2.4}$$

where $\gamma_r = \frac{4}{3}$.

Notice that the last three energy equations in the system (2.1) are written in the non-conservative form, which brings much difficulty to the design of a conservative numerical method. To facilitate the design of high order finite difference schemes which could keep the conservation of mass, momentum and total energy, we follow the strategy proposed in our previous paper [7] and introduce the following three new "energy" variables,

$$E_e = \rho e_e + \frac{1}{6}\rho(u^2 + v^2),\ E_i = \rho e_i + \frac{1}{6}\rho(u^2 + v^2),\ E_r = \rho e_r + \frac{1}{6}\rho(u^2 + v^2),$$

and then rewrite (2.1) as

$$\begin{cases}
\partial_t \rho + \nabla \cdot (\rho \mathbf{w}) = 0 \\
\partial_t \rho u + \nabla \cdot (\rho u \mathbf{w}) + \partial_x p = 0 \\
\partial_t \rho v + \nabla \cdot (\rho v \mathbf{w}) + \partial_y p = 0 \\
\partial_t E_e + \nabla \cdot ((E_e + p_e)\mathbf{w}) - \frac{\mathbf{w}}{3} \cdot \nabla (2p_e - p_i - p_r) = \nabla \cdot (\kappa_e \nabla T_e) - \omega_{ei}(T_e - T_i) - \omega_{er}(T_e^4 - T_r^4) \\
\partial_t E_i + \nabla \cdot ((E_i + p_i)\mathbf{w}) - \frac{\mathbf{w}}{3} \cdot \nabla (2p_i - p_e - p_r) = \nabla \cdot (\kappa_i \nabla T_i) + \omega_{ei}(T_e - T_i) \\
\partial_t E_r + \nabla \cdot ((E_r + p_r)\mathbf{w}) - \frac{\mathbf{w}}{3} \cdot \nabla (2p_r - p_e - p_i) = \nabla \cdot (\kappa_r \nabla T_r) + \omega_{er}(T_e^4 - T_r^4)
\end{cases} \tag{2.5}$$

We rewrite the left hand side of the system (2.5) as

$$\frac{\partial \mathbf{U}}{\partial t} + A\frac{\partial \mathbf{U}}{\partial x} + B\frac{\partial \mathbf{U}}{\partial y} = 0,$$

where $\mathbf{U} = (\rho, \rho u, \rho v, E_e, E_i, E_r)^T$, If we consider the γ-law gas (2.3), then A and B which are the Jacobian matrices related to the convection terms are given by,

$$A = \begin{pmatrix}
0 & 1 & 0 & 0 & 0 & 0 \\
\frac{\gamma-9}{6}u^2 + \frac{\gamma-3}{6}v^2 & \frac{9-\gamma}{3}u & \frac{3-\gamma}{3}v & \gamma_e - 1 & \gamma_i - 1 & \gamma_r - 1 \\
-uv & v & u & 0 & 0 & 0 \\
-\gamma_e e_e u + \frac{\gamma-6}{18}uw^2 & \gamma_e e_e + \frac{v^2}{6} + \frac{9-2\gamma}{18}u^2 & \frac{3-\gamma}{9}uv & \frac{\gamma_e+2}{3}u & \frac{\gamma_i-1}{3}u & \frac{\gamma_r-1}{3}u \\
-\gamma_i e_i u + \frac{\gamma-6}{18}uw^2 & \gamma_i e_i + \frac{v^2}{6} + \frac{9-2\gamma}{18}u^2 & \frac{3-\gamma}{9}uv & \frac{\gamma_e-1}{3}u & \frac{\gamma_i+2}{3}u & \frac{\gamma_r-1}{3}u \\
-\gamma_r e_r u + \frac{\gamma-6}{18}uw^2 & \gamma_r e_r + \frac{v^2}{6} + \frac{9-2\gamma}{18}u^2 & \frac{3-\gamma}{9}uv & \frac{\gamma_e-1}{3}u & \frac{\gamma_i-1}{3}u & \frac{\gamma_r+2}{3}u
\end{pmatrix}, \tag{2.6}$$

$$B = \begin{pmatrix}
0 & 0 & 1 & 0 & 0 & 0 \\
-uv & v & u & 0 & 0 & 0 \\
\frac{\gamma-9}{6}v^2 + \frac{\gamma-3}{6}u^2 & \frac{3-\gamma}{3}u & \frac{9-\gamma}{3}v & \gamma_e - 1 & \gamma_i - 1 & \gamma_r - 1 \\
-\gamma_e e_e v + \frac{\gamma-6}{18}vw^2 & \frac{3-\gamma}{9}uv & \gamma_e e_e + \frac{u^2}{6} + \frac{9-2\gamma}{18}v^2 & \frac{\gamma_e+2}{3}v & \frac{\gamma_i-1}{3}v & \frac{\gamma_r-1}{3}v \\
-\gamma_i e_i v + \frac{\gamma-6}{18}vw^2 & \frac{3-\gamma}{9}uv & \gamma_i e_i + \frac{u^2}{6} + \frac{9-2\gamma}{18}v^2 & \frac{\gamma_e-1}{3}v & \frac{\gamma_i+2}{3}v & \frac{\gamma_r-1}{3}v \\
-\gamma_r e_r v + \frac{\gamma-6}{18}vw^2 & \frac{3-\gamma}{9}uv & \gamma_r e_r + \frac{u^2}{6} + \frac{9-2\gamma}{18}v^2 & \frac{\gamma_e-1}{3}v & \frac{\gamma_i-1}{3}v & \frac{\gamma_r+2}{3}v
\end{pmatrix}, \tag{2.7}$$

where $w = \sqrt{u^2 + v^2}$, $\gamma = \gamma_e + \gamma_i + \gamma_r$.

2.1 Eigenvalues and eigenvectors of A and B.

The eigenvalues of A are

$$\{u - c_s, u, u, u, u, u + c_s\}$$

where c_s is the sound speed given by

$$c_s = \sqrt{\gamma_e(\gamma_e - 1)e_e + \gamma_i(\gamma_i - 1)e_i + \gamma_r(\gamma_r - 1)e_r}. \tag{2.8}$$

The corresponding right eigenvectors to A are as follows,

$$R_A^{(1)} = \begin{pmatrix} 1 \\ u - c_s \\ v \\ \gamma_e e_e + \frac{w^2}{6} - \frac{uc_s}{3} \\ \gamma_i e_i + \frac{w^2}{6} - \frac{uc_s}{3} \\ \gamma_r e_r + \frac{w^2}{6} - \frac{uc_s}{3} \end{pmatrix}, \quad R_A^{(2)} = \begin{pmatrix} 1 \\ u \\ v \\ \frac{g_t w^2}{6 g_e} \\ g_r \\ -g_i \end{pmatrix}, \quad R_A^{(3)} = \begin{pmatrix} 1 \\ u \\ v \\ -g_r \\ \frac{g_t w^2}{6 g_i} \\ g_e \end{pmatrix},$$

$$R_A^{(4)} = \begin{pmatrix} 1 \\ u \\ v \\ g_i \\ -g_e \\ \frac{g_t w^2}{6 g_r} \end{pmatrix}, \quad R_A^{(5)} = \begin{pmatrix} 0 \\ 0 \\ 1 \\ \frac{v}{3} \\ \frac{v}{3} \\ \frac{v}{3} \end{pmatrix}, \quad R_A^{(6)} = \begin{pmatrix} 1 \\ u + c_s \\ v \\ \gamma_e e_e + \frac{w^2}{6} + \frac{uc_s}{3} \\ \gamma_i e_i + \frac{w^2}{6} + \frac{uc_s}{3} \\ \gamma_r e_r + \frac{w^2}{6} + \frac{uc_s}{3} \end{pmatrix}.$$

The left eigenvectors of the matrix A can be written in the following form,

$$L_A^{(1)} = \frac{1}{12c_s^2} \begin{pmatrix} g_t w^2 + 6uc_s \\ -2g_t u - 6c_s \\ -2g_t v \\ 6g_e \\ 6g_i \\ 6g_r \end{pmatrix}, \quad L_A^{(2)} = \begin{pmatrix} \frac{g_e}{g_t} - \frac{g_e w^2}{6c_s^2} - \frac{g_e g_t w^2}{b}(H_e - c_s^2 w^2) \\ \frac{g_e u}{3c_s^2} + \frac{2g_e g_t u}{b}(H_e - c_s^2 w^2) \\ \frac{g_e v}{3c_s^2} + \frac{2g_e g_t v}{b}(H_e - c_s^2 w^2) \\ -\frac{g_e^2}{g_t c_s^2} - \frac{6g_e}{b}(g_e H_e - g_t c_s^2 w^2) \\ -\frac{g_e g_i}{g_t c_s^2} - \frac{6g_e g_i}{b}(H_e - 6g_r c_s^2) \\ -\frac{g_e g_r}{g_t c_s^2} - \frac{6g_e g_r}{b}(H_e + 6g_i c_s^2) \end{pmatrix},$$

$$L_A^{(3)} = \begin{pmatrix} \frac{g_i}{g_t} - \frac{g_i w^2}{6c_s^2} - \frac{g_i g_t w^2}{b}(H_i - c_s^2 w^2) \\ \frac{g_i u}{3c_s^2} + \frac{2g_i g_t u}{b}(H_i - c_s^2 w^2) \\ \frac{g_i v}{3c_s^2} + \frac{2g_i g_t v}{b}(H_i - c_s^2 w^2) \\ -\frac{g_i g_e}{g_t c_s^2} - \frac{6g_i g_e}{b}(H_i + 6g_r c_s^2) \\ -\frac{g_i^2}{g_t c_s^2} - \frac{6g_i}{b}(g_i H_i - g_t c_s^2 w^2) \\ -\frac{g_i g_r}{g_t c_s^2} - \frac{6g_i g_r}{b}(H_i - 6g_e c_s^2) \end{pmatrix}, \quad L_A^{(4)} = \begin{pmatrix} \frac{g_r}{g_t} - \frac{g_r w^2}{6c_s^2} - \frac{g_r g_t w^2}{b}(H_r - c_s^2 w^2) \\ \frac{g_r u}{3c_s^2} + \frac{2g_r g_t u}{b}(H_r - c_s^2 w^2) \\ \frac{g_r v}{3c_s^2} + \frac{2g_r g_t v}{b}(H_r - c_s^2 w^2) \\ -\frac{g_r g_e}{g_t c_s^2} - \frac{6g_r g_e}{b}(H_r - 6g_i c_s^2) \\ -\frac{g_r g_i}{g_t c_s^2} - \frac{6g_r g_i}{b}(H_r + 6g_e c_s^2) \\ -\frac{g_r^2}{g_t c_s^2} - \frac{6g_r}{b}(g_r H_r - g_t c_s^2 w^2) \end{pmatrix},$$

$$L_A^{(5)} = \begin{pmatrix} -v \\ 0 \\ 1 \\ 0 \\ 0 \\ 0 \end{pmatrix}, \quad L_A^{(6)} = \frac{1}{12c_s^2} \begin{pmatrix} g_t w^2 - 6uc_s \\ -2g_t u + 6c_s \\ -2g_t v \\ 6g_e \\ 6g_i \\ 6g_r \end{pmatrix}.$$

where

$$g_t = \gamma_e + \gamma_i + \gamma_r - 3,$$

$$g_e = \gamma_e - 1, \quad g_i = \gamma_i - 1, \quad g_r = \gamma_r - 1,$$

$$H_e = 6g_i g_r \left(\gamma_i e_i - \gamma_r e_r\right) + \gamma_e g_t e_e w^2,$$

$$H_i = 6g_e g_r \left(\gamma_r e_r - \gamma_e e_e\right) + \gamma_i g_t e_i w^2,$$

$$H_r = 6g_e g_i \left(\gamma_e e_e - \gamma_i e_i\right) + \gamma_r g_t e_r w^2,$$

$$b = g_t \left(36 g_e g_i g_r + g_t w^4\right) c_s^2.$$

(2.9)

In the same way, the eigenvalues of B are

$$\{v - c_s, v, v, v, v, v + c_s\}$$

with the corresponding right eigenvectors

$$R_B^{(1)} = \begin{pmatrix} 1 \\ u \\ v - c_s \\ \gamma_e e_e + \frac{w^2}{6} - \frac{v c_s}{3} \\ \gamma_i e_i + \frac{w^2}{6} - \frac{v c_s}{3} \\ \gamma_r e_r + \frac{w^2}{6} - \frac{v c_s}{3} \end{pmatrix}, \quad R_B^{(2)} = \begin{pmatrix} 0 \\ 1 \\ 0 \\ \frac{u}{3} \\ \frac{u}{3} \\ \frac{u}{3} \end{pmatrix}, \quad R_B^{(3)} = \begin{pmatrix} 1 \\ u \\ v \\ \frac{g_t w^2}{6 g_e} \\ g_r \\ -g_i \end{pmatrix},$$

$$R_B^{(4)} = \begin{pmatrix} 1 \\ u \\ v \\ -g_r \\ \frac{g_t w^2}{6 g_i} \\ g_e \end{pmatrix}, \quad R_B^{(5)} = \begin{pmatrix} 1 \\ u \\ v \\ g_i \\ -g_e \\ \frac{g_t w^2}{6 g_r} \end{pmatrix}, \quad R_B^{(6)} = \begin{pmatrix} 1 \\ u \\ v + c_s \\ \gamma_e e_e + \frac{w^2}{6} + \frac{v c_s}{3} \\ \gamma_i e_i + \frac{w^2}{6} + \frac{v c_s}{3} \\ \gamma_r e_r + \frac{w^2}{6} + \frac{v c_s}{3} \end{pmatrix},$$

and the left eigenvectors of the matrix B can be written in the following form,

$$L_B^{(1)} = \frac{1}{12 c_s^2} \begin{pmatrix} g_t w^2 + 6 v c_s \\ -2 g_t u \\ -2 g_t v - 6 c_s \\ 6 g_e \\ 6 g_i \\ 6 g_r \end{pmatrix}, \quad L_B^{(2)} = \begin{pmatrix} -u \\ 1 \\ 0 \\ 0 \\ 0 \\ 0 \end{pmatrix}, \quad L_B^{(3)} = \begin{pmatrix} \frac{g_e}{g_t} - \frac{g_e w^2}{6 c_s^2} - \frac{g_e g_t w^2}{b}\left(H_e - c_s^2 w^2\right) \\ \frac{g_e u}{3 c_s^2} + \frac{2 g_e g_t u}{b}\left(H_e - c_s^2 w^2\right) \\ \frac{g_e v}{3 c_s^2} + \frac{2 g_e g_t v}{b}\left(H_e - c_s^2 w^2\right) \\ -\frac{g_e^2}{g_t c_s^2} - \frac{6 g_e}{b}\left(g_e H_e - g_t c_s^2 w^2\right) \\ -\frac{g_e g_i}{g_t c_s^2} - \frac{6 g_e g_i}{b}\left(H_e - 6 g_r c_s^2\right) \\ -\frac{g_e g_r}{g_t c_s^2} - \frac{6 g_e g_r}{b}\left(H_e + 6 g_i c_s^2\right) \end{pmatrix},$$

$$L_B^{(4)} = \begin{pmatrix} \frac{g_i}{g_t} - \frac{g_i w^2}{6 c_s^2} - \frac{g_i g_t w^2}{b}\left(H_i - c_s^2 w^2\right) \\ \frac{g_i u}{3 c_s^2} + \frac{2 g_i g_t u}{b}\left(H_i - c_s^2 w^2\right) \\ \frac{g_i v}{3 c_s^2} + \frac{2 g_i g_t v}{b}\left(H_i - c_s^2 w^2\right) \\ -\frac{g_i g_e}{g_t c_s^2} - \frac{6 g_i g_e}{b}\left(H_i + 6 g_r c_s^2\right) \\ -\frac{g_i^2}{g_t c_s^2} - \frac{6 g_i}{b}\left(g_i H_i - g_t c_s^2 w^2\right) \\ -\frac{g_i g_r}{g_t c_s^2} - \frac{6 g_i g_r}{b}\left(H_i - 6 g_e c_s^2\right) \end{pmatrix}, \quad L_B^{(5)} = \begin{pmatrix} \frac{g_r}{g_t} - \frac{g_r w^2}{6 c_s^2} - \frac{g_r g_t w^2}{b}\left(H_r - c_s^2 w^2\right) \\ \frac{g_r u}{3 c_s^2} + \frac{2 g_r g_t u}{b}\left(H_r - c_s^2 w^2\right) \\ \frac{g_r v}{3 c_s^2} + \frac{2 g_r g_t v}{b}\left(H_r - c_s^2 w^2\right) \\ -\frac{g_r g_e}{g_t c_s^2} - \frac{6 g_r g_e}{b}\left(H_r - 6 g_i c_s^2\right) \\ -\frac{g_r g_i}{g_t c_s^2} - \frac{6 g_r g_i}{b}\left(H_r + 6 g_e c_s^2\right) \\ -\frac{g_r^2}{g_t c_s^2} - \frac{6 g_r}{b}\left(g_r H_r - g_t c_s^2 w^2\right) \end{pmatrix},$$

7

$$L_B^{(6)} = \frac{1}{12c_s^2} \begin{pmatrix} g_t w^2 - 6vc_s \\ -2g_t u \\ -2g_t v + 6c_s \\ 6g_e \\ 6g_i \\ 6g_r \end{pmatrix}.$$

The information of these left and right eigenvalues will be applied in the characteristic decomposition for the high order WENO approximation that we will introduce in the next section.

3 High order conservative finite difference WENO scheme for the 1D 3-T RH equations

The 1D 3-T RH equations can be written as,

$$\frac{\partial \mathbf{U}}{\partial t} = -\frac{\partial \mathbf{F}}{\partial x} + \frac{u}{3}\frac{\partial \mathbf{N}}{\partial x} + \frac{\partial \mathbf{G}}{\partial x} + \mathbf{S} \tag{3.1}$$

where the vectors of the evolving variables $\mathbf{U}$, the conservative convection term $\mathbf{F}$, the non-conservative convection term $\mathbf{N}$, the diffusion term $\mathbf{G}$ and the energy-exchange term $\mathbf{S}$ are given by

$$\mathbf{U} = \begin{pmatrix} \rho \\ \rho u \\ E_e \\ E_i \\ E_r \end{pmatrix}, \qquad \mathbf{F} = \begin{pmatrix} \rho u \\ \rho u^2 + p \\ (E_e + p_e)u \\ (E_i + p_i)u \\ (E_r + p_r)u \end{pmatrix}, \qquad \mathbf{N} = \begin{pmatrix} 0 \\ 0 \\ 2p_e - p_i - p_r \\ 2p_i - p_e - p_r \\ 2p_r - p_e - p_i \end{pmatrix},$$

$$\mathbf{G} = \begin{pmatrix} 0 \\ 0 \\ \kappa_e \partial_x T_e \\ \kappa_i \partial_x T_i \\ \kappa_r \partial_x T_r^4 \end{pmatrix}, \qquad \mathbf{S} = \begin{pmatrix} 0 \\ 0 \\ -\omega_{ei}(T_e - T_i) - \omega_{er}(T_e^4 - T_r^4) \\ \omega_{ei}(T_e - T_i) \\ \omega_{er}(T_e^4 - T_r^4) \end{pmatrix}. \tag{3.2}$$

3.1 High order spatial discretization

Let $\{x_j, j = 1, ..., N_x\}$ be a uniform mesh of the computational domain $[a, b]$, with the mesh size $\Delta x = \frac{b-a}{N_x-1}$. The variables are defined at x_j identified by the subscript j. The semi discrete finite difference scheme for the system (3.1)-(3.2) is given as,

$$\frac{d\mathbf{U}_j(t)}{dt} = -\frac{\left(\hat{\mathbf{F}}_{j+1/2} - \hat{\mathbf{F}}_{j-1/2}\right)}{\Delta x} + \mathcal{N}_j + \left(\frac{\partial \mathbf{G}}{\partial x}\right)_j + \mathbf{S}_j \tag{3.3}$$

8

where $\mathbf{U}_j(t), \mathcal{N}_j, \left(\frac{\partial \mathbf{G}}{\partial x}\right)_j, \mathbf{S}_j$ are the numerical approximations to the point values of $\mathbf{U}(x_j, t_n)$, $\left(\frac{u}{3}\frac{\partial \mathbf{N}}{\partial x}\right)(x_j, t_n), \left(\frac{\partial \mathbf{G}}{\partial x}\right)(x_j, t_n), \mathbf{S}(x_j, t_n)$ respectively, and the numerical flux

$$\hat{\mathbf{F}}_{j+1/2} = \hat{\mathbf{F}}(\mathbf{U}_{j-r}, ..., \mathbf{U}_{j+s}),$$

where $r = 2$ and $s = 3$ for the fifth order WENO scheme that we use in this paper, should satisfy the following conditions:

- $\hat{\mathbf{F}}$ is a Lipschitz continuous function in all the arguments;

- $\hat{\mathbf{F}}$ is consistent with the physical flux $\mathbf{F}$, that is, $\hat{\mathbf{F}}(u, ..., u) = \mathbf{F}(u)$.

Next we will discuss the specific procedures to determine the individual terms in the semi-discrete scheme (3.3).

3.1.1 The determination of the conservative convection term

We first discuss how to discretize the conservative convection term $\hat{\mathbf{F}}$ in the scheme (3.3). Denote the eigenvalues of $\mathbf{F}'(\mathbf{U}_j)$ as $\lambda_j^1, ..., \lambda_j^5$, and take the maximum as $\alpha_1 = \max_j |\lambda_j^1|, ..., \alpha_5 = \max_j |\lambda_j^5|$, and finally $\alpha = \max_{1 \leq \ell \leq 5} \alpha_\ell$.

We perform a local characteristic decomposition and apply the scalar WENO algorithm in each characteristic direction, to avoid spurious oscillations near discontinuities.

The algorithm is summarized as follows:

Algorithm 3.1.

1. Find the Roe average of $\mathbf{U}_j$ and $\mathbf{U}_{j+1}$ denoted by $\mathbf{U}_{j+\frac{1}{2}}$, the Jacobian $\mathbf{F}'(\mathbf{U}_{j+\frac{1}{2}})$ and its right and left eigenvector matrices $\mathbf{R}$ and $\mathbf{L}$.

2. Project $\mathbf{F}_\ell$ and $\mathbf{U}_\ell$, for $\ell = j - r, ..., j + s$, to local characteristic directions,

$$\tilde{\mathbf{F}}_\ell = \mathbf{L}\mathbf{F}_\ell, \qquad \tilde{\mathbf{U}}_\ell = \mathbf{L}\mathbf{U}_\ell.$$

3. Compute
$$\tilde{\mathbf{F}}_\ell^{\pm} = \frac{1}{2}(\tilde{\mathbf{F}}_\ell \pm diag(\alpha_1, ..., \alpha_5)\tilde{\mathbf{U}}_\ell), \qquad \ell = j - r, ..., j + s, \tag{3.4}$$
where $diag(\alpha_1, ..., \alpha_5)$ is the diagonal matrix with the maximum eigenvalues on its diagonal line.

4. Apply the scalar WENO algorithm [12] to each component of $\tilde{\mathbf{F}}_\ell^{\pm}$ to obtain $\tilde{\mathbf{F}}_{j+\frac{1}{2}}^{\pm}$, and then obtain $\tilde{\mathbf{F}}_{j+\frac{1}{2}} = \tilde{\mathbf{F}}_{j+\frac{1}{2}}^{+} + \tilde{\mathbf{F}}_{j+\frac{1}{2}}^{-}$.

5. Project back to component space $\hat{\mathbf{F}}_{j+\frac{1}{2}} = \mathbf{R}\tilde{\mathbf{F}}_{j+\frac{1}{2}}$.

3.1.2 The determination of the nonconservative convection term

The non-conservative convection term $\mathcal{N}_j$ is discretized in the way [8] which was proposed for Hamilton-Jacobi equations,

$$\mathcal{N}_j = \frac{u_j}{3}\left(\frac{\partial \mathbf{N}}{\partial x}\right)_j + [\mathbf{N}]_{j-\frac{1}{2}} + [\mathbf{N}]_{j+\frac{1}{2}} \tag{3.5}$$

where

$$[\mathbf{N}]_{j-\frac{1}{2}} = \frac{1}{3}\max\{u_{j-1}, u_j, 0\}\begin{pmatrix} 0 \\ 0 \\ [2p_e - p_i - p_r]_{j-\frac{1}{2}} \\ [2p_i - p_e - p_r]_{j-\frac{1}{2}} \\ [2p_r - p_e - p_i]_{j-\frac{1}{2}} \end{pmatrix}, \tag{3.6}$$

$$[\mathbf{N}]_{j+\frac{1}{2}} = \frac{1}{3}\min\{u_j, u_{j+1}, 0\}\begin{pmatrix} 0 \\ 0 \\ [2p_e - p_i - p_r]_{j+\frac{1}{2}} \\ [2p_i - p_e - p_r]_{j+\frac{1}{2}} \\ [2p_r - p_e - p_i]_{j+\frac{1}{2}} \end{pmatrix}. \tag{3.7}$$

Here, $[q]_{j+\frac{1}{2}} = q_{j+\frac{1}{2}}^+ - q_{j+\frac{1}{2}}^-$, $q_{j+\frac{1}{2}}^- = q_j(x_{j+\frac{1}{2}})$, $q_{j-\frac{1}{2}}^+ = q_j(x_{j-\frac{1}{2}})$, and $q_j(x)$ is the interpolation polynomial of q by the information of point values at $x_{j-3}, x_{j-2}, ..., x_{j+2}, x_{j+3}$ with $q = p_e, p_i, p_r$ respectively.

The $((p_e)_x)_j$, $((p_i)_x)_j$, $((p_r)_x)_j$ used in the term $\left(\frac{\partial \mathbf{N}}{\partial x}\right)_j$ are determined by,

$$(q_x)_j = \frac{q_{j+3} - 9q_{j+2} + 45q_{j+1} - 45q_{j-1} + 9q_{j-2} - q_{j-3}}{60\Delta x} \tag{3.8}$$

with $q = p_e, p_i, p_r$ respectively.

Of course, we could also use WENO interpolation for these non-conservative terms, at a slightly higher computational cost. However, it appears that using the simple interpolation here does not lead to noticeable spurious oscillations in the numerical tests in this paper.

3.1.3 The determination of the energy-exchange term

The energy-exchange term $\mathbf{S}_j$ in the scheme (3.3) is given by

$$\mathbf{S}_j = \begin{pmatrix} 0 \\ 0 \\ -\omega_{ei}((T_e)_j - (T_i)_j) - \omega_{er}((T_e^4)_j - (T_r^4)_j) \\ \omega_{ei}((T_e)_j - (T_i)_j) \\ \omega_{er}((T_e^4)_j - (T_r^4)_j) \end{pmatrix}. \tag{3.9}$$

where $(T_e)_j, (T_i)_j, (T_r)_j$ are computed by $\mathbf{U}_j$.

3.1.4 The determination of the diffusion term

We use the following formulas to determine $\partial_x(\kappa_e\partial_x T_e), \partial_x(\kappa_i\partial_x T_i), \partial_x(\kappa_r\partial_x T_r^4)$ in the diffusion term $\mathbf{G}$,

$$\partial_x(\kappa_s\partial_x q)_j = \frac{\kappa_s\left(2q_{j+3} - 27q_{j+2} + 270q_{j+1} - 490q_j + 270q_{j-1} - 27q_{j-2} + 2q_{j-3}\right)}{180\Delta x^2} \quad (3.10)$$

with $(s,q) = (e, T_e), (i, T_i), (r, T_r^4)$ respectively.

Again, we could also use WENO approximations for the diffusion term, at a slightly higher computational cost. However, it appears that using the simple central difference approximations here does not lead to noticeable spurious oscillations in the numerical tests in this paper.

Remark: The semi discrete scheme (3.3) can keep the conservation of mass, momentum and total energy. We refer to [7] for a similar proof and will not repeat it here.

3.2 The high order Runge-Kutta time discretization

To design a finite difference scheme with high order accuracy both in space and time, the time marching is implemented by a third order total variation diminishing (TVD), or strong stability preserving (SSP) Runge-Kutta type method [16, 11], which has the following form.

$$\begin{aligned}
\mathbf{U}_j^{(1)} &= \mathbf{U}_j^n + \Delta t\mathbf{L}(\mathbf{U}^n)_j, \\
\mathbf{U}_j^{(2)} &= \frac{3}{4}\mathbf{U}_j^n + \frac{1}{4}\Delta t\big(\mathbf{U}_j^{(1)} + \mathbf{L}(\mathbf{U}^{(1)})_j\big), \\
\mathbf{U}_j^{n+1} &= \frac{1}{3}\mathbf{U}_j^n + \frac{2}{3}\Delta t\big(\mathbf{U}_j^{(2)} + \mathbf{L}(\mathbf{U}^{(2)})_j\big),
\end{aligned} \quad (3.11)$$

where $\mathbf{L}$ is the numerical spatial operator representing the right hand of the scheme (3.3).

3.3 The time step for the high order finite difference WENO scheme solving the 1D 3-T RH equations

For the explicit finite difference scheme (3.11), the time step is limited by the three terms of the 3-T RH equations, namely, the convection term, the diffusion term and the energy-exchange term [7],

$$\Delta t \leq \min_{j=1,\dots,N_x} \frac{\lambda}{\nu_j}, \qquad \nu_j = \frac{(c_s)_j}{\Delta x} + \frac{2d_j}{\Delta x^2} + s_j \quad (3.12)$$

where λ is a positive constant less than 1, which is chosen as 0.5 in this paper. $(c_s)_j$ is defined by (2.8).

$$d_j = \max\{\frac{\kappa_e}{c_{ve}\rho_j}, \frac{\kappa_i}{c_{vi}\rho_j}, \frac{\kappa_r}{a}\}, \quad s_j = \max\{|(\alpha_1)_j|, |(\alpha_2)_j|\}. \quad (3.13)$$

where

$$\alpha_1 = \frac{-s_1 + s_2}{s}, \quad \alpha_2 = \frac{s_1 + s_2}{s} \tag{3.14}$$

with

$$s_1 = \sqrt{\left(a\omega_{ei}c_{ve}^4 + a\omega_{ei}c_{ve}^3 c_{vi} + 4a\omega_{er}c_{vi}e_e^3 + \omega_{er}c_{ve}^4 c_{vi}\rho\right)^2 - 4a\omega_{ei}\omega_{er}c_{ve}^4 c_{vi}\left(4ae_e^3 + c_{ve}^4\rho + c_{ve}^3 c_{vi}\rho\right)},$$

$$s_2 = -(a\omega_{ei}c_{ve}^4 + a\omega_{ei}c_{ve}^3 c_{vi} + 4a\omega_{er}c_{vi}e_e^3 + \omega_{er}c_{ve}^4 c_{vi}\rho),$$

$$s = 2ac_{ve}^4 c_{vi}\rho.$$

4 High order conservative finite difference WENO scheme for the 2D 3-T RH equations

We rewrite the 2D 3-T RH equations (2.5) in the following form,

$$\frac{\partial \mathbf{U}}{\partial t} = -\frac{\partial \mathbf{F}^1}{\partial x} - \frac{\partial \mathbf{F}^2}{\partial y} + \frac{u}{3}\frac{\partial \mathbf{N}}{\partial x} + \frac{v}{3}\frac{\partial \mathbf{N}}{\partial y} + \frac{\partial \mathbf{G}^1}{\partial x} + \frac{\partial \mathbf{G}^2}{\partial y} + \mathbf{S} \tag{4.1}$$

where the vectors of the evolving variables $\mathbf{U}$, the conservative convection terms $\mathbf{F}^1, \mathbf{F}^2$, the non-conservative convection term $\mathbf{N}$, the diffusion terms $\mathbf{G}^1, \mathbf{G}^2$ and the energy-exchange term $\mathbf{S}$ are defined as,

$$\mathbf{U} = \begin{pmatrix} \rho \\ \rho u \\ \rho v \\ E_e \\ E_i \\ E_r \end{pmatrix}, \qquad \mathbf{F}^1 = \begin{pmatrix} \rho u \\ \rho u^2 + p \\ \rho uv \\ (E_e + p_e)u \\ (E_i + p_i)u \\ (E_r + p_r)u \end{pmatrix}, \qquad \mathbf{F}^2 = \begin{pmatrix} \rho v \\ \rho uv \\ \rho v^2 + p \\ (E_e + p_e)v \\ (E_i + p_i)v \\ (E_r + p_r)v \end{pmatrix},$$

$$\mathbf{N} = \begin{pmatrix} 0 \\ 0 \\ 0 \\ 2p_e - p_i - p_r \\ 2p_i - p_e - p_r \\ 2p_r - p_e - p_i \end{pmatrix}, \qquad \mathbf{G}^1 = \begin{pmatrix} 0 \\ 0 \\ 0 \\ \kappa_e \partial_x T_e \\ \kappa_i \partial_x T_i \\ \kappa_r \partial_x T_r^4 \end{pmatrix}, \qquad \mathbf{G}^2 = \begin{pmatrix} 0 \\ 0 \\ 0 \\ \kappa_e \partial_y T_e \\ \kappa_i \partial_y T_i \\ \kappa_r \partial_y T_r^4 \end{pmatrix}, \tag{4.2}$$

$$\mathbf{S} = \begin{pmatrix} 0 \\ 0 \\ 0 \\ -\omega_{ei}(T_e - T_i) - \omega_{er}(T_e^4 - T_r^4) \\ \omega_{ei}(T_e - T_i) \\ \omega_{er}(T_e^4 - T_r^4) \end{pmatrix}.$$

Suppose the rectangular computational domain $[a, b] \times [c, d]$ is divided by the $N_x \times N_y$ uniform points. $\Delta x = \frac{b-a}{N_x-1}, \Delta y = \frac{d-c}{N_y-1}$. Then the semi discrete high order finite difference scheme for the 2D 3-T RH system (4.1)-(4.2) could be given in the following way,

$$\frac{d\mathbf{U}_{j,k}(t)}{dt} = -\frac{\left(\hat{\mathbf{F}}^1_{j+1/2,k} - \hat{\mathbf{F}}^1_{j-1/2,k}\right)}{\Delta x} - \frac{\left(\hat{\mathbf{F}}^2_{j,k+1/2} - \hat{\mathbf{F}}^2_{j,k-1/2}\right)}{\Delta y} \\ + \mathcal{N}_{j,k} + \left(\frac{\partial \mathbf{G}^1}{\partial x}\right)_{j,k} + \left(\frac{\partial \mathbf{G}^2}{\partial y}\right)_{j,k} + \mathbf{S}_{j,k} \tag{4.3}$$

The definition of the variables in (4.3) is similar as those in (3.3). One main advantage of the finite difference scheme is that we can use the 1D algorithm in each direction to compute the derivative in that direction. In particular, the numerical fluxes $\hat{\mathbf{F}}^1_{j+\frac{1}{2},k}$ and $\hat{\mathbf{F}}^2_{j,k+\frac{1}{2}}$ can be obtained as follows.

Algorithm 4.1

1. For $k = 1, 2, ... N_y$, denote $\mathbf{W}_j = \mathbf{U}_{j,k}$, $\hat{\mathbf{F}}_j = \hat{\mathbf{F}}^1_{j,k}$, then perform the one dimensional Algorithm 3.1 using $\mathbf{W}_j$ and $\hat{\mathbf{F}}_j$ to obtain the numerical flux $\hat{\mathbf{F}}^1_{j+\frac{1}{2},k}$.

2. For $j = 1, 2, ... N_x$, denote $\mathbf{W}_k = \mathbf{U}_{j,k}$, $\hat{\mathbf{F}}_k = \hat{\mathbf{F}}^2_{j,k}$, then perform the one dimensional Algorithm 3.1 using $\mathbf{W}_k$ and $\hat{\mathbf{F}}_k$ to obtain the numerical flux $\hat{\mathbf{F}}^2_{j,k+\frac{1}{2}}$.

The other terms such as $\mathcal{N}_{j,k}, \left(\frac{\partial \mathbf{G}^1}{\partial x}\right)_{j,k}, \left(\frac{\partial \mathbf{G}^2}{\partial y}\right)_{j,k}, \mathbf{S}_{j,k}$ in (4.3) can be given in the similar way as those in the 1D finite difference scheme (3.3). The similar high order SSP Runge-Kutta type method (3.11) is adopted for the time discretization.

5 Numerical results

In this section, we perform some numerical experiments on our fifth order finite difference schemes solving the 3-T RH equations (3.1)-(3.2) and (4.1)-(4.2) respectively. The c_{ve}, c_{vi} and the radiation constant a are taken to be 1 unless otherwise stated. The reference solutions for the following discontinuous problems are obtained by grid-refinement converged numerical solutions.

5.1 1D numerical results

Example 5.1 (1D accuracy test).

First we use the manufactured solution for the 1D system (3.1)-(3.2) proposed in [7] to test the accuracy of our 1D fifth order finite difference WENO scheme with the third order

Table 5.1: Errors and orders for Example 5.1 performed by the fifth order finite difference scheme solving 1D 3-T RH equations (3.1)-(3.2) at $T = 1$

N	L	ρ	order	ρu	order	E_e	order	E_i	order	E_r	order
20	L_1	1.41E-3		1.89E-3		3.87E-3		4.11E-3		3.26E-3	
	L_∞	4.25E-3		5.55E-3		1.57E-2		1.36E-2		1.83E-2	
40	L_1	1.14E-4	3.62	7.94E-5	4.58	3.17E-4	3.61	3.58E-4	3.52	2.69E-4	3.60
	L_∞	5.39E-4	2.98	1.96E-4	4.83	1.23E-3	3.68	1.69E-3	3.01	8.30E-4	4.46
80	L_1	4.08E-6	4.81	2.50E-6	4.99	1.12E-5	4.82	1.19E-5	4.91	5.12E-6	5.71
	L_∞	2.57E-5	4.39	1.82E-5	3.43	5.21E-5	4.56	7.20E-5	4.55	2.07E-5	5.32
160	L_1	1.16E-7	5.14	7.77E-8	5.00	3.10E-7	5.17	3.33E-7	5.16	1.40E-7	5.20
	L_∞	8.05E-7	5.00	5.82E-7	4.96	1.53E-6	5.09	2.10E-6	5.10	6.04E-7	5.10
320	L_1	2.85E-9	5.34	2.08E-9	5.22	7.58E-9	5.35	8.30E-9	5.33	3.76E-9	5.21
	L_∞	2.30E-8	5.13	2.95E-8	4.30	4.51E-8	5.09	5.48E-8	5.26	2.34E-8	4.69

SSP Runge-Kutta time discretizaiton. We design the problem to have the following exact solutions by adding the adequate artificial source terms to the system (3.1)-(3.2),

$$\begin{cases} \rho(x,t) = 1 + 0.5\sin(x+t) \\ u(x,t) = 2 + \cos(x+t) \\ \rho e_e(x,t) = 3(1 + 0.2\cos(x+t)) \\ \rho e_i(x,t) = 3(1 + 0.2\sin(x+t)) \\ \rho e_r(x,t) = 2(1 + 0.1\cos(x+t)) \end{cases} . \tag{5.1}$$

The computational domain is $[0, 2\pi]$. $\gamma_e = \gamma_i = \frac{5}{3}$. $w_{ei} = w_{er} = 1$. $\kappa_e = \kappa_i = \kappa_r = 1$. In this test, the periodic boundary condition is applied.

Table 5.1 shows the errors and orders for the our fifth order finite difference scheme. In the table, we observe that the scheme achieves fifth order accuracy both in L_1 and L_∞ norms for all the variables we solve.

Next we perform some 1D non-oscillatory tests [7] to verify the high-resolution and non-oscillatory properties of our finite difference scheme.

Example 5.2 (The 3-T double Lax radiation shock tube problem).

In this and the next tests, in order to treat the boundary condition easily, we duplicate the 3-T wave symmetrically and extend it periodically so that we can adopt the periodic boundary conditions at the boundaries. For this problem, the computational domain is [-10, 30]. The initial condition is as follows,

$$\begin{cases} \rho = 0.445, & u = 0.698, & p_e = p_i = p_r = 1.176, & -10 \le x < 0 \\ \rho = 0.5, & u = 0, & p_e = p_i = p_r = 0.19, & 0 \le x < 20 \\ \rho = 0.445, & u = 0.698, & p_e = p_i = p_r = 1.176, & 20 \le x \le 30 \end{cases} \tag{5.2}$$

$\gamma_e = \gamma_i = \frac{5}{3}$. The periodic boundary condition is applied. The results of our fifth order finite difference scheme using 400 uniform grid points compared with the reference solution at $T =$

1 are shown in Figures 5.1-5.2. In Figure 5.1, we give the numerical results of ρ, u, T_e, T_i, T_r obtained by our fifth order finite difference scheme solving the 3-T RH equations (3.1)-(3.2) without the diffusion and energy-exchange terms, i.e., $w_{ei} = w_{er} = 0$ and $\kappa_e = \kappa_i = \kappa_r = 0$. From the figures, we notice that the scheme can capture the shocks and contacts sharply, and there is no noticeable spurious oscillation near the discontinuities. The results coincide with the reference solution well. We next present the numerical results of our scheme solving the 3-T RH equations (3.1)-(3.2) with the diffusion and energy-exchange terms in Figure 5.2, where $w_{ei} = w_{er} = 1$ and $\kappa_e = \kappa_i = \kappa_r = 1$. The images look more smooth due to the effect of diffusion. The electron, ion and radiation possess different temperatures at the final time since the energy-exchange terms are enacted.
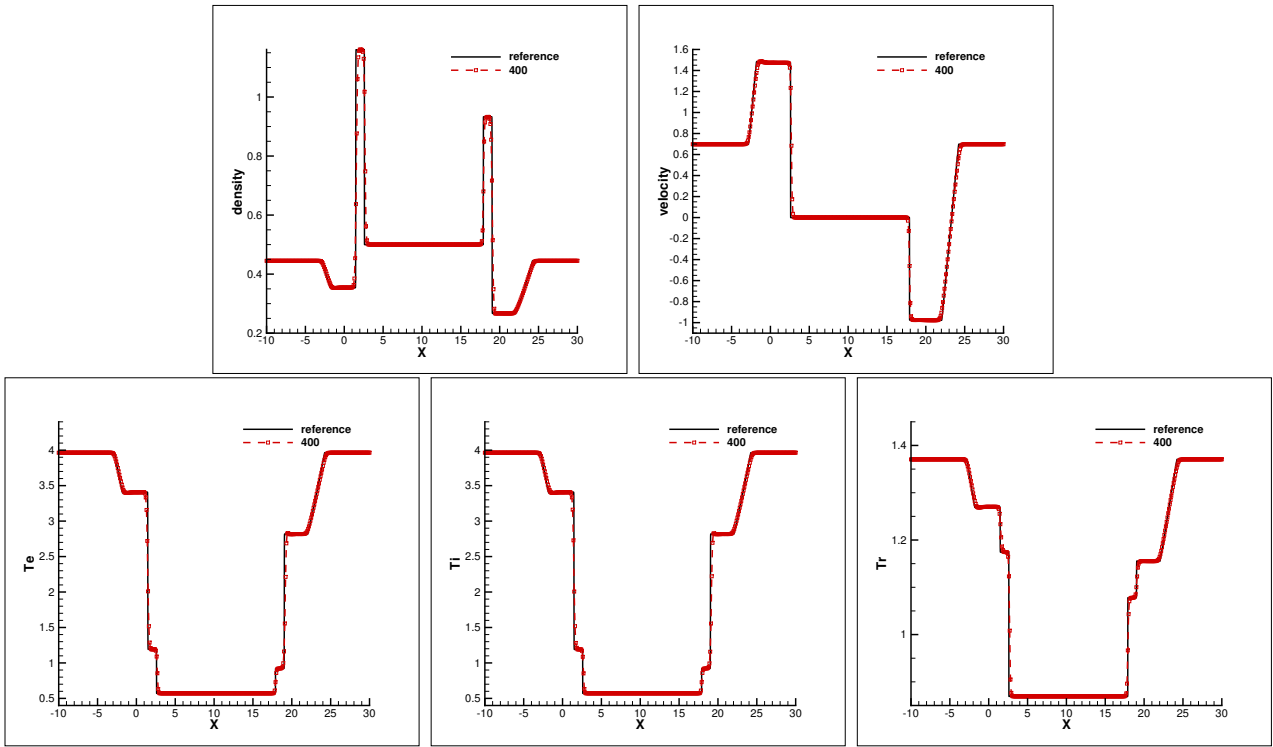
Figure 5.1: The numerical results for Example 5.2 at $T = 1$ by the fifth order finite difference scheme solving the 1D 3-T RH equations (3.1)-(3.2) without the diffusion and energy-exchange terms on the 400 grid against the reference solution at $T = 1$ by using the fifth order finite difference scheme solving the 3-T RH equations Left and Top: density, Right and Top: velocity, Left and Bottom: electron temperature, Middle and Bottom: ion temperature, Right and Bottom: radiation temperature.
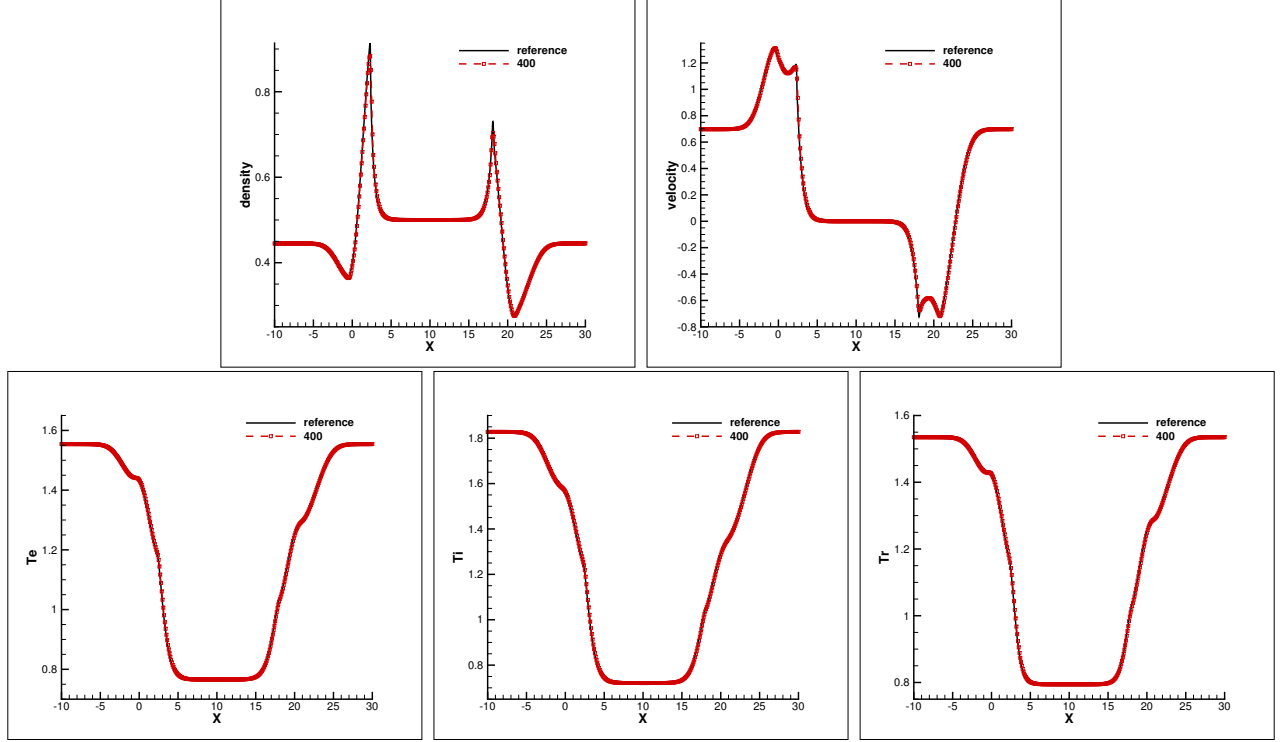
Figure 5.2: The numerical results for Example 5.2 at $T = 1$ by the fifth order finite difference scheme solving the 1D 3-T RH equations (3.1)-(3.2) with $w_{ei} = w_{er} = 1$ and $\kappa_e = \kappa_i = \kappa_r = 1$ on the 400 grid. Left and Top: density, Right and Top: velocity, Left and Bottom: electron temperature, Middle and Bottom: ion temperature, Right and Bottom: radiation temperature.

Example 5.3 (The 3-T RH problem of double two-interacting blast waves).

In this 3-T RH problem of double two-interacting blast waves, the computational domain is $[0, 2]$. The initial condition is taken as,

$$\rho = 1, \quad u = 0, \quad p = \begin{cases} 1000, & 0 \leq x < 0.1 \\ 0.01, & 0.1 \leq x < 0.9 \\ 100, & 0.9 \leq x < 1.1 \\ 0.01, & 1.1 \leq x < 1.9 \\ 1000, & 1.9 \leq x \leq 2 \end{cases}, \quad p_e = p_i = p_r = \frac{1}{3}p. \quad (5.3)$$

$\gamma_e = \gamma_i = 1.4$. $w_{ei} = w_{er} = 0$. $\kappa_e = \kappa_i = 0.01, \kappa_r = 0.001$. The periodic boundary condition is applied. The results of our fifth order finite difference scheme solving the 3-T RH equations (3.1)-(3.2) with 800 uniform grid points against the reference solution at $T = 0.038$ are shown in Figure 5.3. We can observe the scheme can capture the fine structures well and there is no noticeable spurious oscillation near the strong shocks and contacts.
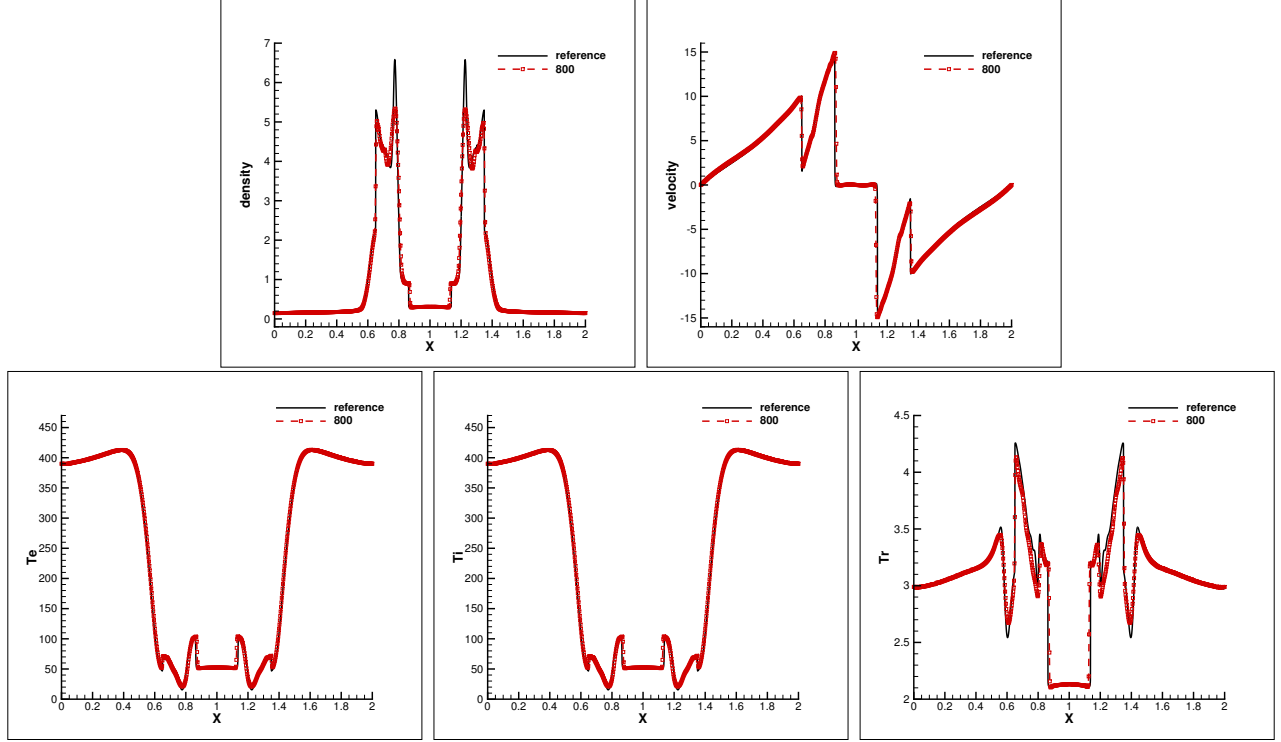
Figure 5.3: The numerical results for Example 5.3 at $T = 0.038$ by the fifth order finite difference scheme solving the 1D 3-T RH equations (3.1)-(3.2) on the 800 grid. Left and Top: density, Right and Top: velocity, Left and Bottom: electron temperature, Middle and Bottom: ion temperature, Right and Bottom: radiation temperature.

Example 5.4 (The 3-T radiation shock tube problem involving two rarefaction waves).

In this problem, there are two rarefaction waves moving towards the opposite directions. Its initial condition is as follows,

$$\begin{cases} \rho = 1, & u = -1, & p_e = p_i = p_r = 1, & -2 \leq x < 0 \\ \rho = 1, & u = 1, & p_e = p_i = p_r = 1, & 0 \leq x \leq 2 \end{cases} \tag{5.4}$$

with $\gamma_e = \gamma_i = \frac{5}{3}$. $w_{ei} = w_{er} = 0$. We test this problem with the different conduction coefficients, that is, $\kappa = \kappa_e = \kappa_i = \kappa_r = 0, 0.1, 0.5, 1$ respectively. The Dirichlet boundary condition is adopted at the left and right boundaries. Figure 5.4 shows the results of our fifth order finite difference scheme by using 400 grid points at $T = 0.2$. We observe the difference of the solution with the change of the conduction coefficients. Consistently with common physical sense, the diffusion effect is more obvious with the increasing $\kappa_e, \kappa_i, \kappa_r$.
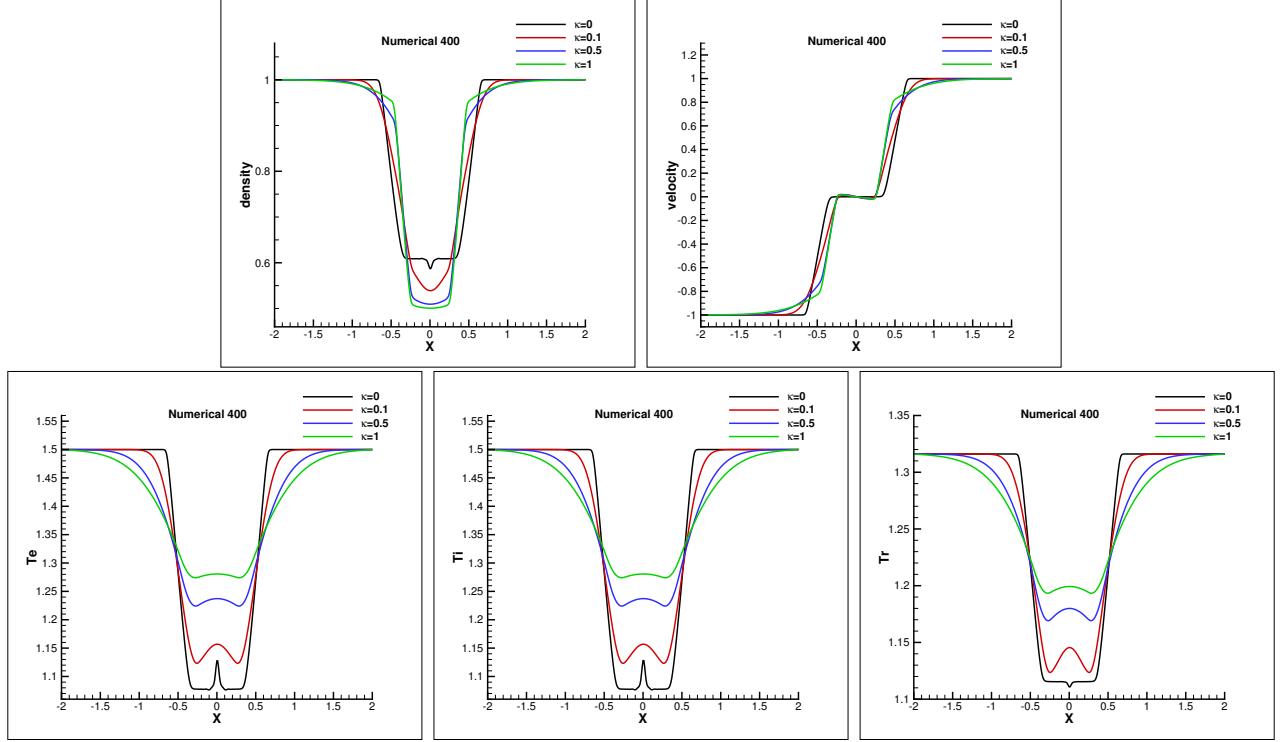
Figure 5.4: The numerical results for Example 5.4 at $T = 0.2$ by the fifth order finite difference scheme solving the 3-T RH equations (3.1)-(3.2) with the different $\kappa_e, \kappa_i, \kappa_r$ on the 400 grid. Left and Top: density, Right and Top: velocity, Left and Bottom: electron temperature, Middle and Bottom: ion temperature, Right and Bottom: radiation temperature.

5.2   2D numerical results

Example 5.5 (2D accuracy test).

Next, we test the accuracy of our two-dimensional finite difference scheme solving the system (4.1)-(4.2). We use the 2D manufactured solution introduced in [7] to perform the test. The exact solution for this test is as follows,

$$\begin{cases} \rho(x, y, t) = 1 + 0.5 \sin(x + y - 2t) \\ u(x, y, t) = v(x, y, t) = 2 + \cos(x + y - 2t) \\ \rho e_e(x, y, t) = 3(1 + 0.2 \sin(x + y - 2t)) \\ \rho e_i(x, y, t) = 3(1 + 0.2 \cos(x + y - 2t)) \\ \rho e_r(x, y, t) = 2(1 + 0.1 \sin(x + y - 2t)) \end{cases} \quad . \tag{5.5}$$

$\gamma_e = \gamma_i = \frac{5}{3}$. $w_{ei} = w_{er} = 0.1$. $\kappa_e = \kappa_i = \kappa_r = 0.1$. The computational domain is $[0, 2\pi] \times [0, 2\pi]$ which is uniformly divided into $N_x \times N_y$ grid points. The periodic boundary condition is applied at four boundaries. Table 5.2 shows the errors and orders of our 2D finite difference scheme where we notice our 2D scheme possesses fifth-order accuracy both in L_1 and L_∞ norms for the variables $\rho, \rho u, \rho v, E_e, E_i, E_r$ which we solve directly.

Table 5.2: Errors and orders for Example 5.5 performed by the fifth order finite difference scheme solving the 2D 3-T RH equations (4.1)-(4.2) at $T = 1$

$N_x = N_y$	L	ρ	k	ρu	k	ρv	k	E_e	k	E_i	k	E_r	k
20	L_1	5.20E-03		8.42E-03		8.42E-03		1.61E-02		1.45E-02		1.38E-02	
	L_∞	1.53E-02		3.09E-02		3.09E-02		5.60E-02		4.73E-02		3.80E-02	
40	L_1	2.21E-04	4.56	2.91E-04	4.85	2.91E-04	4.85	6.79E-04	4.57	7.10E-04	4.35	6.30E-04	4.45
	L_∞	6.72E-04	4.51	1.57E-03	4.30	1.57E-03	4.30	2.16E-03	4.69	3.73E-03	3.67	2.56E-03	3.89
80	L_1	6.10E-06	5.18	9.74E-06	4.90	9.74E-06	4.90	1.95E-05	5.12	2.04E-05	5.13	2.06E-05	4.93
	L_∞	3.14E-05	4.42	9.23E-05	4.09	9.23E-05	4.09	1.06E-04	4.35	1.76E-04	4.40	9.02E-05	4.83
160	L_1	1.80E-07	5.08	2.77E-07	5.14	2.77E-07	5.14	5.46E-07	5.16	6.29E-07	5.02	6.57E-07	4.97
	L_∞	9.27E-07	5.08	3.83E-06	4.59	3.83E-06	4.59	2.89E-06	5.20	4.69E-06	5.23	2.46E-06	5.20
320	L_1	5.27E-09	5.10	9.16E-09	4.92	9.16E-09	4.92	1.65E-08	5.05	1.78E-08	5.14	1.89E-08	5.12
	L_∞	3.77E-08	4.62	1.89E-07	4.35	1.89E-07	4.35	9.10E-08	4.99	1.40E-07	5.07	8.55E-08	4.85

Next we will test several 2D 3-T RH problems with large fluid distortion, which can not be simulated by the pure Lagrangian method.

Example 5.6 (The interaction of a 3-T RH shock wave with a bubble).

Next, we study a 3-T RH problem involving the interaction of a shock wave with a bubble, which is inspired by a famous pure hydrodynamics problem, that is, the interaction of a shock wave with a helium bubble [5]. The computational domain is $[0, 6.5] \times [0, 0.89]$. The center of the bubble is located at $(x_c, y_c) = (3.5, 0)$ with a radius $r = 0.5$. Since our scheme can not treat the multi-material problem so far, we take the bubble with the same γ as the fluid, specifically $\gamma_e = \gamma_i = 1.4$. We then modify the initial value of pressure inside the bubble to mimic the similar behavior of the bubble's deformation. The initial state of the bubble is $(\rho, u, v, p_e, p_i, p_r) = (0.1819, 0, 0, 0.146972, 0.146972, 0.146972)$. The initial condition for the other computational domain is as follows,

$$\begin{cases} \rho = 1, & u = v = 0, & p_e = p_i = p_r = 0.238095, & 0 \le x < 4.5 \\ \rho = 1.3764, & u = -0.3336, & v = 0, & p_e = p_i = p_r = 0.373762, & 4.5 \le x \le 6.5 \end{cases} \quad (5.6)$$

See Figure 5.5 for the initial state of density. The reflective boundary condition is imposed at the bottom and top boundaries. The Dirichlet boundary condition is applied at left and right boundaries. $w_{ei} = w_{er} = 0$ and $\kappa_e = \kappa_i = \kappa_r = 0$. We test this problem by our 2D 3-T fifth order WENO finite difference scheme with 800×288 uniform grid points. The numerical results at $t = 0.6294, 1.1099, 3.3408, 5.0358, 7.1571$ after the incident shock hits the bubble are shown in Figure 5.6. The evolution of the bubble after the shock hitting, deforming and then forming a jet and eventually generating a vortex ring can be observed from our numerical results. The performance of the radiation temperature is quite different from the electron and ion temperatures.
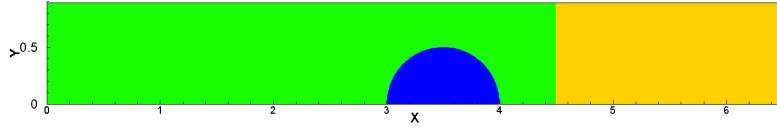
Figure 5.5: The initial condition of density for Example 5.6.
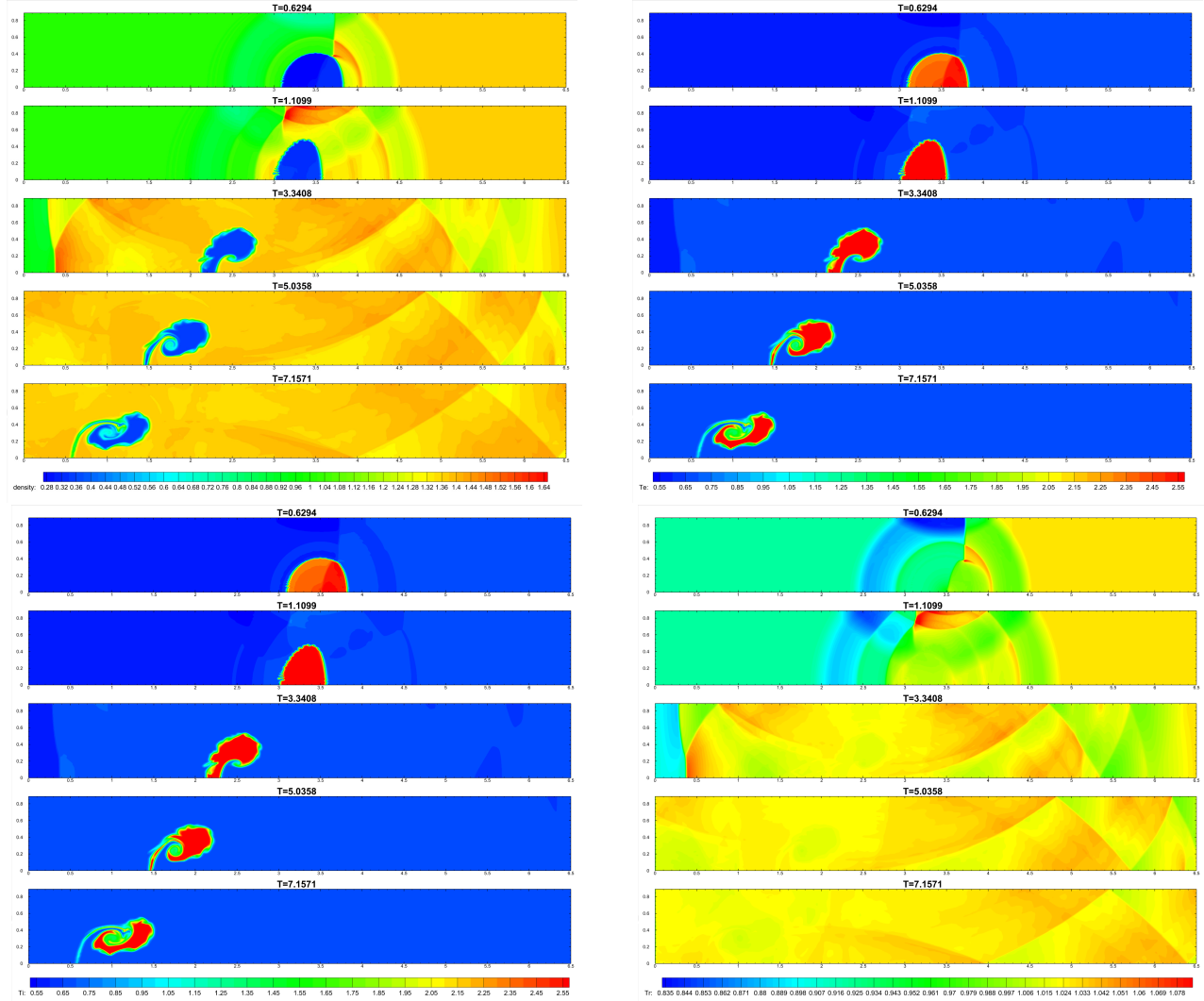
Figure 5.6: The numerical results for Example 5.6 by the fifth order finite difference scheme solving the 2D 3-T RH equations (4.1)-(4.2) at different times on the 800×288 grid. Left and Top: density, Right and Top: electron temperature, Left and Bottom: ion temperature, Right and Bottom: radiation temperature.

Example 5.7 (The second interaction problem of a 3-T RH shock wave with a bubble).

20

Next we test the second interaction problem of a radiation shock wave with a bubble, which is extended from another widely studied pure hydrodynamics interaction test of a shock wave with a helium bubble [4]. The computational domain is $[0, 0.5] \times [-0.089, 0.089]$. The center of the bubble is located at $(x_c, y_c) = (0.32, 0)$ with a radius $r = 0.025$. Similarly as the above test, we take $\gamma_e = \gamma_i = 1.4$ at the whole region. We modify the value of pressure inside the bubble at the initial time to model the similar behavior of the bubble's deformation. The initial state of the bubble is $(\rho, u, v, p_e, p_i, p_r) = (0.182, 0, 0, \frac{p}{3}, \frac{p}{3}, \frac{p}{3})$, where $p = \frac{10^5(\gamma_e-1)}{\gamma_h-1}, \gamma_h = 1.648$. The shock wave is initially located at $x = 0.35$ as,

$$
\begin{cases}
\rho = 1, & u = v = 0, & p_e = p_i = p_r = \frac{100000}{3}, & 0 \le x < 0.35 \\
\rho = 1.376, & u = -124.824, \quad v = 0, & p_e = p_i = p_r = \frac{156980}{3}, & 0.35 \le x \le 0.5
\end{cases}
\tag{5.7}
$$

See Figure 5.7 for the initial condition of density for this test. The reflective boundary condition is imposed at the bottom and top boundaries. The Dirichlet boundary condition is applied at the left and right boundaries. We first test this problem by our 2D 3-T fifth order WENO finite difference scheme with 800×288 uniform grid points solving the system (4.1)-(4.2) without the diffusion and energy-exchange terms, i.e., $w_{ei} = w_{er} = 0$. $\kappa_e = \kappa_i = \kappa_r = 0$. The numerical results of our 2D 3-T RH fifth order WENO finite difference scheme at $t = 1.32 \times 10^{-4}, 4.32 \times 10^{-4}, 6.74 \times 10^{-4}$ and $t = 9.83 \times 10^{-4}$ after the incident shock hits the bubble are shown in Figure 5.8 respectively. From the figures, we can observe that the evolution of the bubble's shape is well captured by our scheme. The numerical results demonstrate the capability of our 3-T-RH high order finite difference scheme in simulating the 3-T radiation hydrodynamics problem with the large fluid deformation.
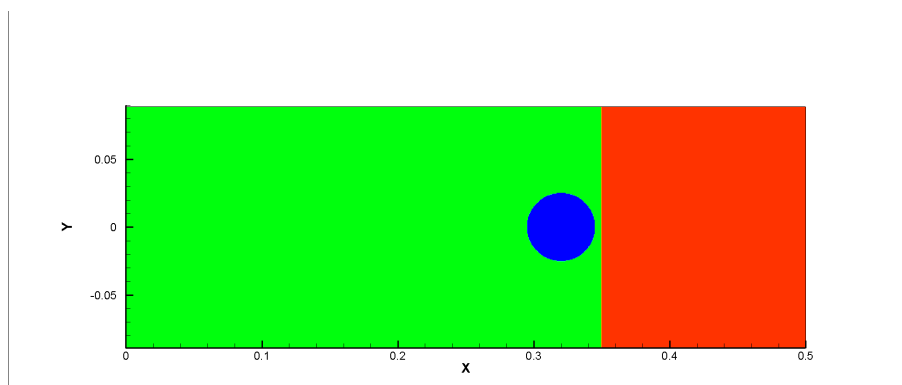
Figure 5.7: The initial condition of density for Example 5.7.
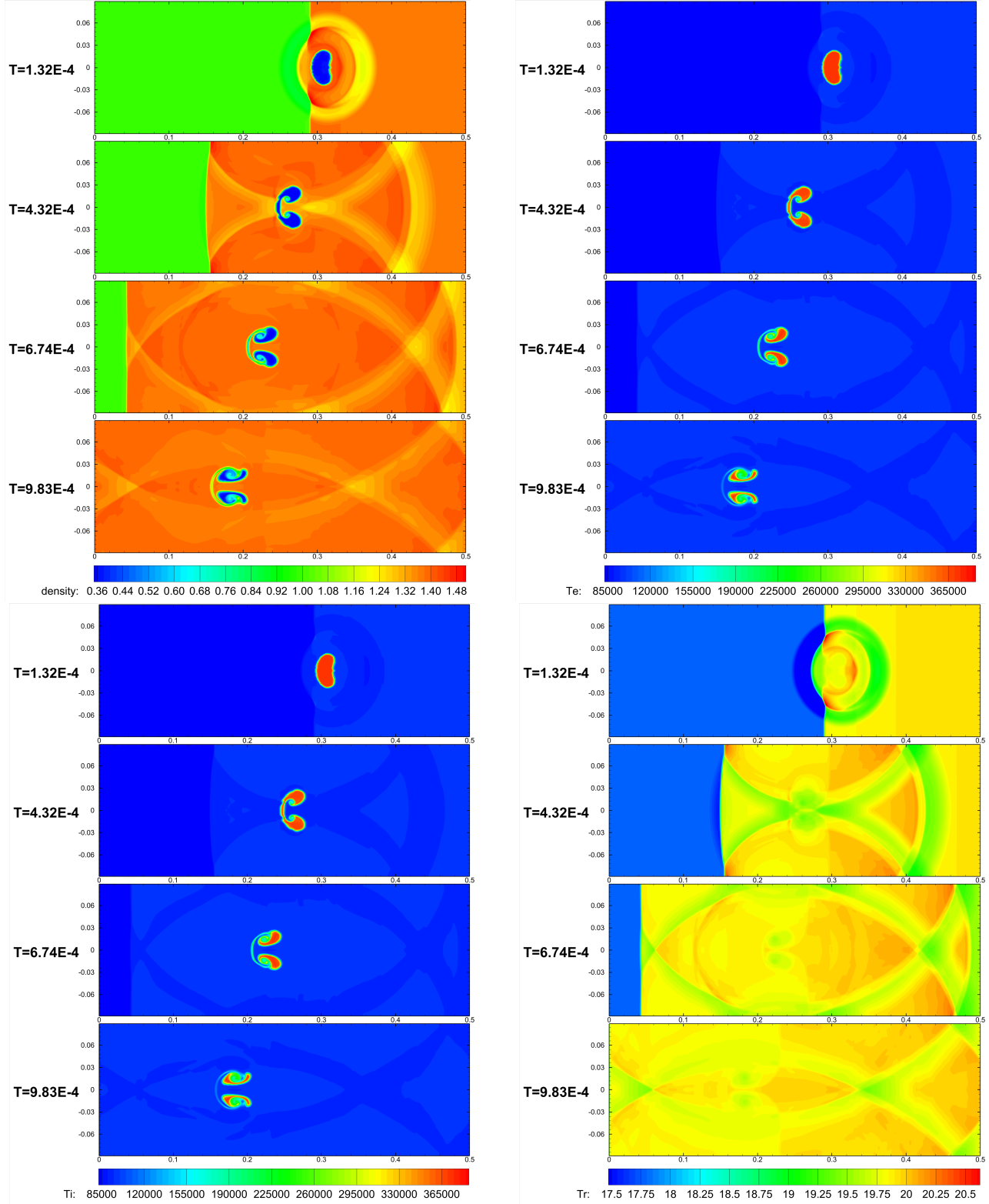
Figure 5.8: The numerical results for Example 5.7 by the fifth order finite difference scheme solving the 2D 3-T RH equations (4.1)-(4.2) with $w_{ei} = w_{er} = 0$ and $\kappa_e = \kappa_i = \kappa_r = 0$ at the different times on the 800×288 grid. Left and Top: density, Right and Top: electron temperature, Left and Bottom: ion temperature, Right and Bottom: radiation temperature.

We further test how the diffusion and energy-exchange terms effect the solution in this problem by our 3-T RH fifth order WENO finite difference scheme solving the system (4.1)-(4.2) with $w_{ei} = 0.05, w_{er} = 0$ and $\kappa_e = \kappa_i = \kappa_r = 0.05$. Figures 5.9 show the results of our scheme at the corresponding different times. Compared with the above results without diffusion and energy-exchange terms, we notice the obvious smear phenomena in the bubble's shape and the quite different images of radiation temperature in these figures.
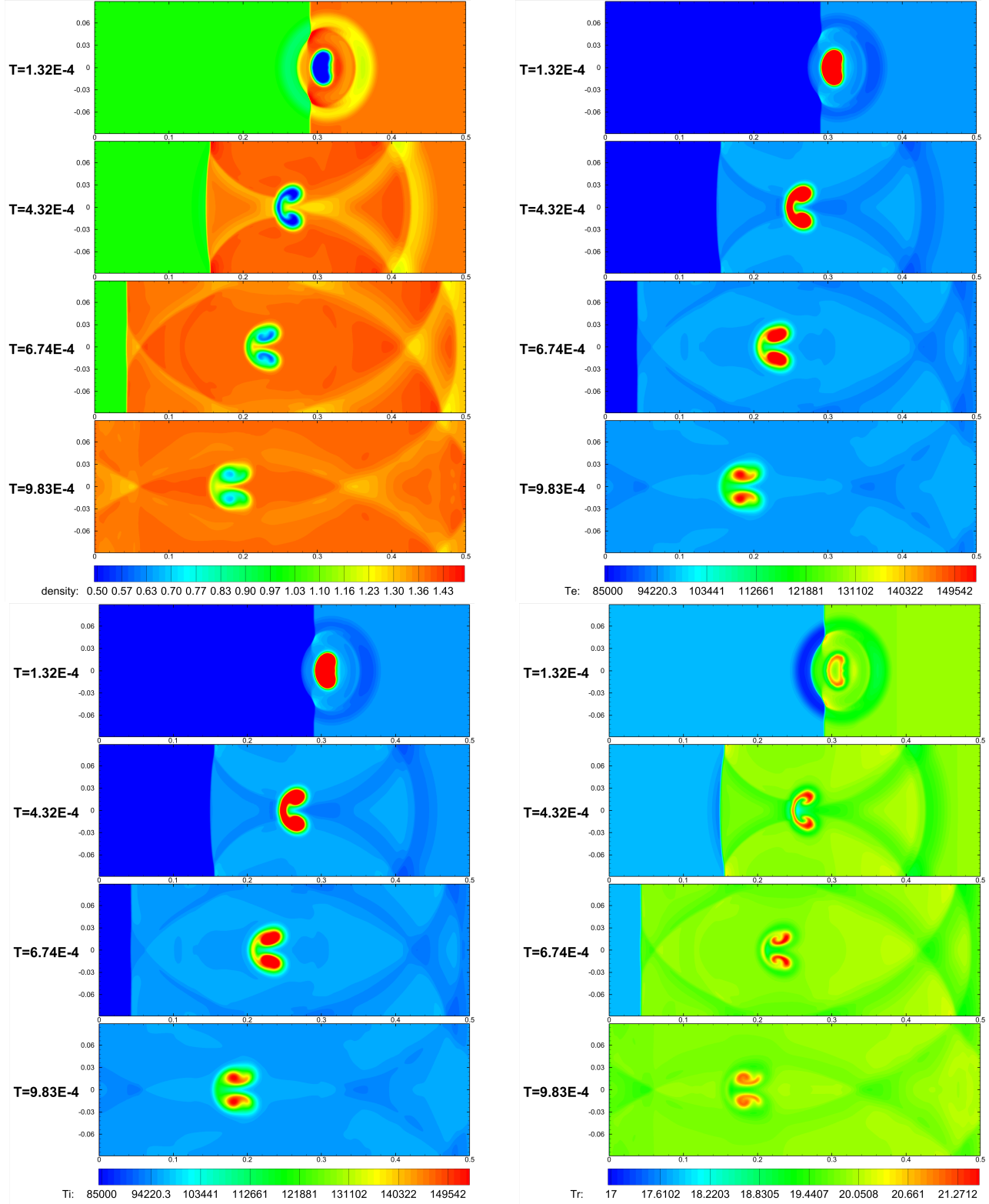
Figure 5.9: The numerical results for Example 5.7 by the fifth order finite difference scheme solving the 2D 3-T RH equations (4.1)-(4.2) with $w_{ei} = 0.05$, $w_{er} = 0$ and $\kappa_e = \kappa_i = \kappa_r = 0.05$ at the different times on the 800×288 grid. Left and Top: density, Right and Top: electron temperature, Left and Bottom: ion temperature, Right and Bottom: radiation temperature.

Example 5.8 (The 3-T Rayleigh-Taylor instability problem).

We design a 3-T radiation hydrodynamic Rayleigh-Taylor instability problem from the originally pure hydrodynamic Rayleigh-Taylor instability problem [19]. The computational domain is $[0, 0.25] \times [0, 1]$. The interface is at $y = 0.5$ at the initial time. The heavy fluid is below the interface, and the light fluid is above the interface with the acceleration in the positive y direction, for which the source term ρ is added to the right-hand side of the third equation and ρv is added to the fifth equation of the system (4.1)-(4.2). A small perturbation is enforced on the y-direction fluid speed at the initial time as,

$$
\begin{cases}
\rho = 2, & u = 0, \quad v = -0.025 c_s \cos(8\pi x), \quad p_e = p_i = p_r = \frac{2y+1}{3}, & 0 \le y < 0.5 \\
\rho = 1, & u = 0, \quad v = -0.025 c_s \cos(8\pi x), \quad p_e = p_i = p_r = \frac{2y+3}{6}, & 0.5 \le y \le 1
\end{cases}
\tag{5.8}
$$

where c_s is the sound speed. $\gamma_e = \gamma_i = \frac{5}{3}$. The reflective boundary conditions are imposed at the left and right boundaries. At the top boundary, the flow values are set as $\rho = 1, u = v = 0, p_e = p_i = p_r = \frac{5}{6}$, and at the bottom boundary the values are $\rho = 2, u = v = 0, p_e = p_i = p_r = \frac{1}{3}$. The final computational time is $T = 1.95$.

The numerical results of our 2D fifth order finite difference WENO scheme solving the 3-T RH equations (4.1)-(4.2) with $w_{ei} = w_{er} = 0$ and $\kappa_e = \kappa_i = \kappa_r = 0$ on the 200×1200 grid are shown in Figure 5.10. We observe that our high order finite difference scheme can capture the small-scale structures in the resolved solutions of density and three temperatures. The non-equilibrium property of electron, ion and radiation is obvious. The radiation has the highest temperature, and the electron plasmas has the smallest temperature.
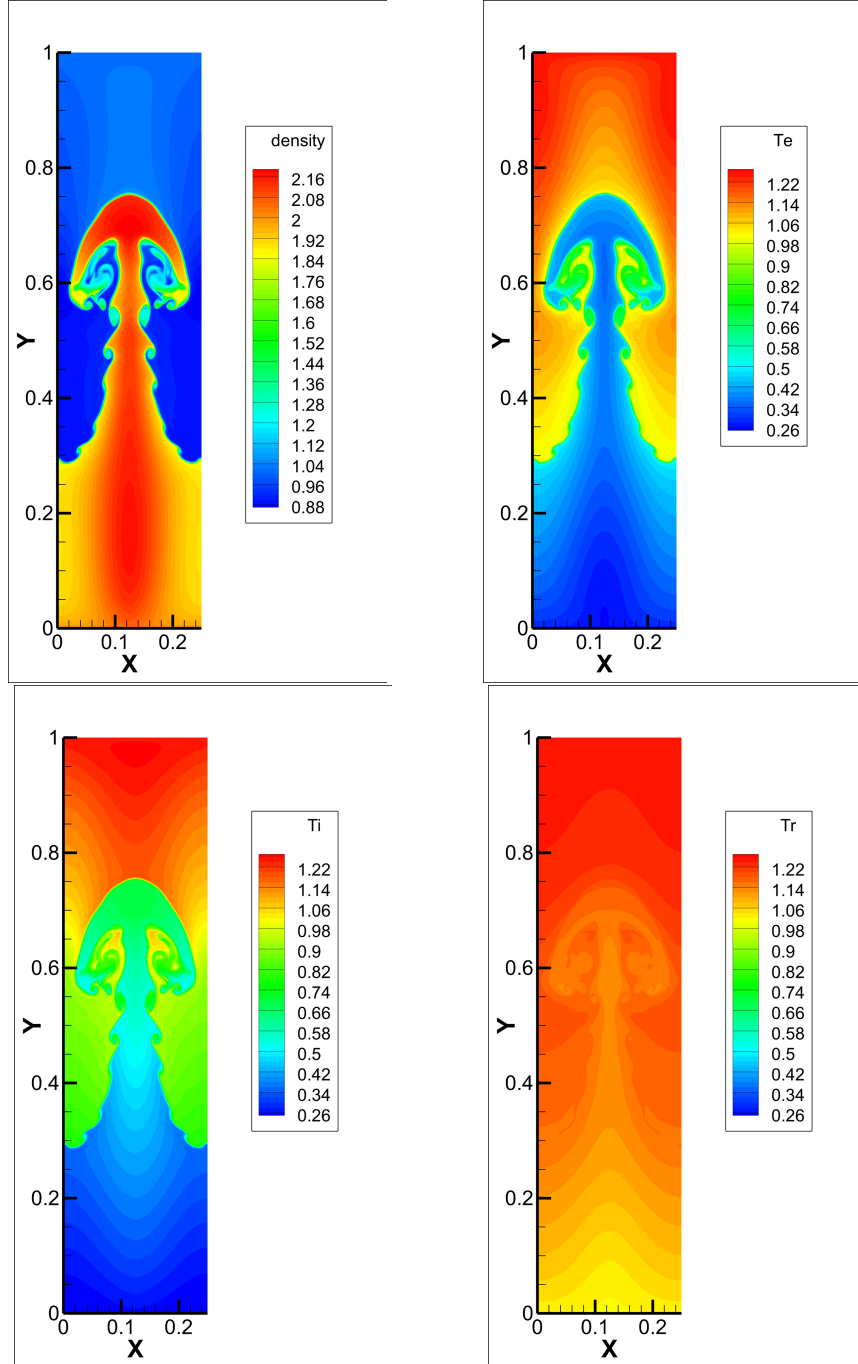
Figure 5.10: The numerical results for Example 5.8 by the fifth order finite difference scheme solving the 2D 3-T RH equations (4.1)-(4.2) at $T = 1.95$ on the 200×1200 grid. Left and Top: density, Right and Top: electron temperature, Left and Bottom: ion temperature, Right and Bottom: radiation temperature.

Example 5.9 (The effects of 3-T RH shock wave on Rayleigh-Taylor instability).

We next introduce a RH shock to hit the above Rayleigh-Taylor interface at a fixed time

$T = 1.6$, and notice the effect of the shock wave when it interacts with the Rayleigh-Taylor (RT) instability flow. For the shock wave hitting the head of the RT interface, we extend the computational domain in the y direction to $[-0.5, 1]$ to avoid the RT interface moving out of the computational domain, that is, the computational domain is $[0, 0.25] \times [-0.5, 1]$. The initial condition for this problem is similar as Example 5.8,

$$\begin{cases} \rho = 2, & u = v = 0, & p_e = p_i = p_r = \frac{1}{3}, & -0.5 \leq y < 0 \\ \rho = 2, & u = 0, \quad v = -0.025c_s \cos(8\pi x), & p_e = p_i = p_r = \frac{3y+1}{3}, & 0 \leq y < 0.5 \\ \rho = 1, & u = 0, \quad v = -0.025c_s \cos(8\pi x), & p_e = p_i = p_r = \frac{2y+3}{6}, & 0.5 \leq y \leq 1 \end{cases} \quad (5.9)$$

The reflective boundary condition is imposed at the left and right boundaries. The boundary condition at $y = -0.5$ is set to be an outflow. At the top boundary, before $T = 1.6$, the flow values are set as $\rho = 1, u = v = 0, p_e = p_i = p_r = \frac{5}{6}$. After $T = 1.6$, the post state of a Mach 6 shock wave is enforced on the top boundary. Figure 5.11 shows the results of our fifth order finite difference scheme solving the 2D 3-T RH equations (4.1)-(4.2) with $w_{ei} = w_{er} = 0$ and $\kappa_e = \kappa_i = \kappa_r = 0$ at three different times $(T = 1.85, 1.9, 2)$ after the shock wave hits the head of Rayleigh-Taylor instability and passes through the Rayleigh-Taylor interface. We can observe that the moving shock wave makes the RT interface move downward. The effect of shock wave speeds up the transition of the RT flow from instability.
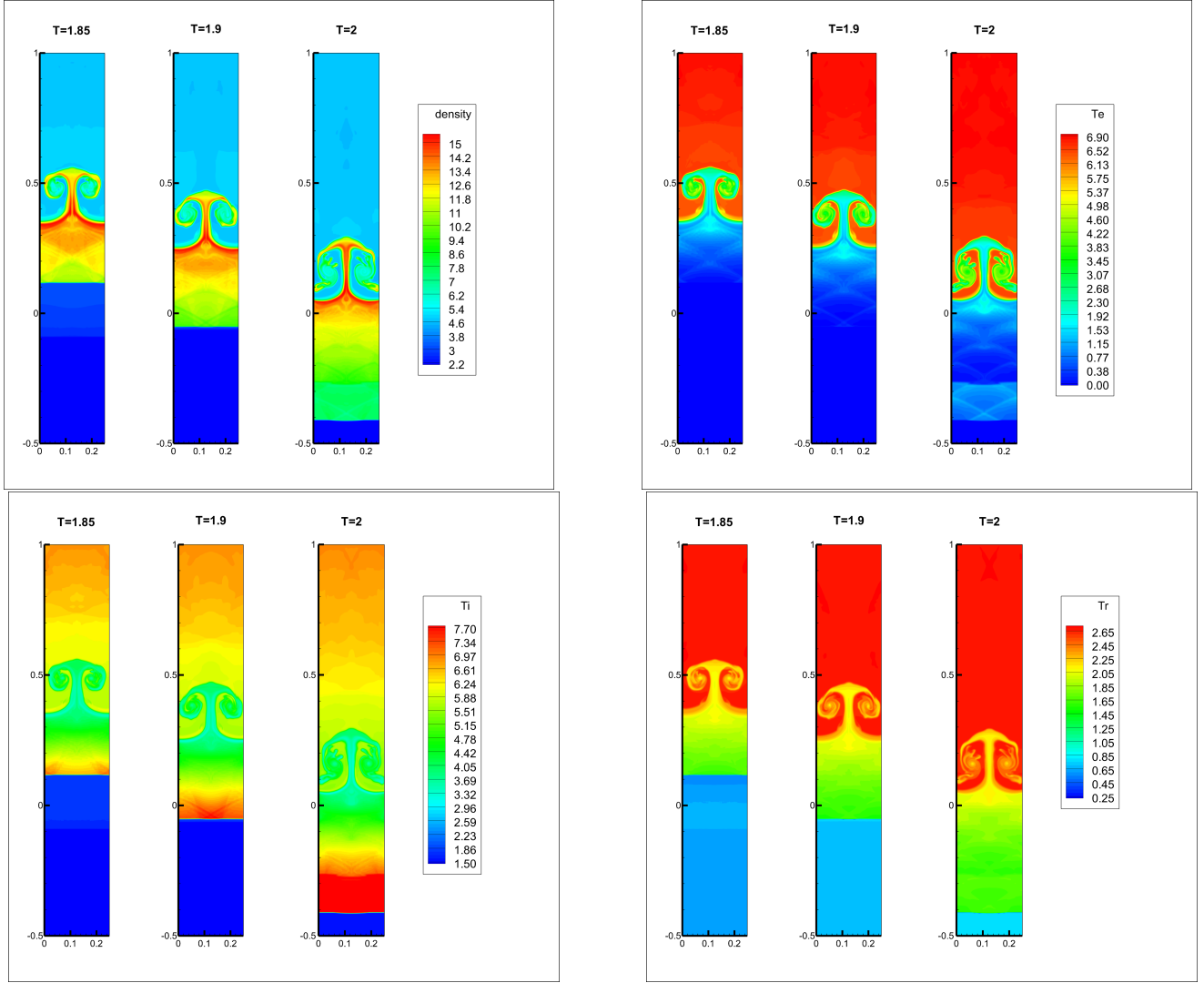
Figure 5.11: The numerical results for Example 5.9 by the fifth order finite difference scheme solving the 2D 3-T RH equations (4.1)-(4.2) with $w_{ei} = w_{er} = 0$ and $\kappa_e = \kappa_i = \kappa_r = 0$ at different times on the 200×1200 grid. Left and Top: density, Right and Top: electron temperature, Left and Bottom: ion temperature, Right and Bottom: radiation temperature.

We further test this problem with the effect of the diffusion and energy-exchange terms. Figures 5.12 show the results of our fifth order finite difference scheme solving the 2D 3-T RH equations (4.1)-(4.2) with $w_{ei} = w_{er} = 0.001$ and $\kappa_e = \kappa_i = \kappa_r = 0.002$ at three different times ($T = 1.85, 1.9, 2$) on the 200×1200 grid. In these figures, we notice that the diffusion and energy-exchange terms make a positive role in preventing the Rayleigh-Taylor flow to instability.

28
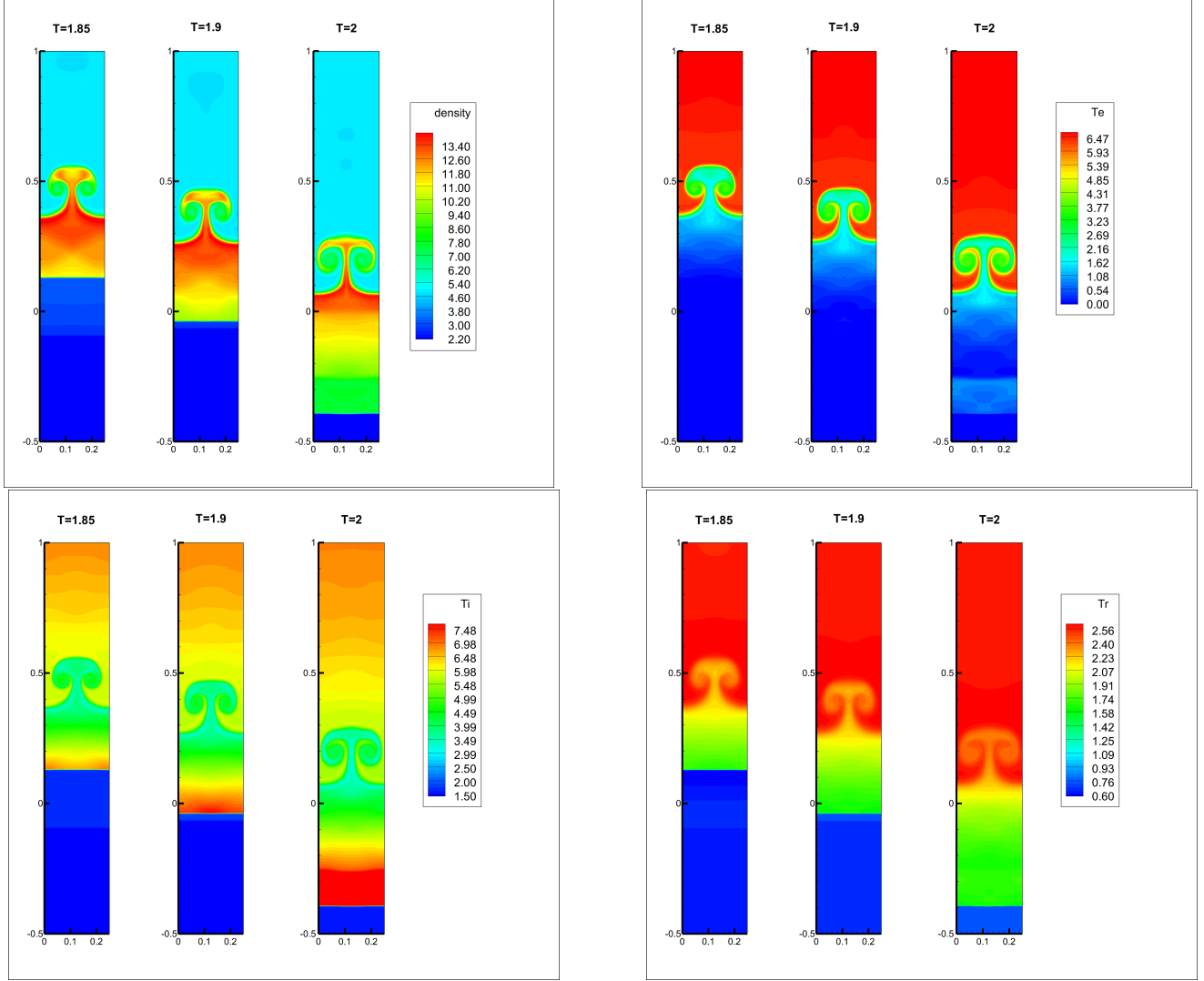
Figure 5.12: The numerical results for Example 5.9 by the fifth order finite difference scheme solving the 2D 3-T RH equations (4.1)-(4.2) with $w_{ei} = w_{er} = 0.001$ and $\kappa_e = \kappa_i = \kappa_r = 0.002$ at the different times on the 200×1200 grid. Left and Top: density, Right and Top: electron temperature, Left and Bottom: ion temperature, Right and Bottom: radiation temperature.

6 Concluding remarks

In this paper, we propose a class of high order conservative finite difference schemes for one-dimensional and two-dimensional three-temperature (3-T) radiation hydrodynamics (RH) equations respectively. We design the finite difference schemes with both high order accuracy and the conservative property by introducing three new energy variables proposed in [7], in the form of which the three energy equations of 3-T RH equations are rewritten. Based on the WENO interpolation and the strong stability preserving (SSP) high order time

discretizations, as an example, we design a class of conservative finite difference schemes with fifth order accuracy in space and third order accuracy in time. Compared with the Lagrangian method we proposed in [7], which can only reach second order accuracy for 2D 3-T RH equations if straight-line edged meshes are used, the finite difference scheme can be easily designed to arbitrary high order accuracy for multi-dimensional 3-T RH equations. The finite difference formulation is also much less expensive in multi-dimensions than the finite volume Lagrangian schemes [7]. Furthermore, it can handle the fluid with large deformation easily. Several 1D and 2D numerical tests are given to demonstrate the good properties of our high order finite difference schemes such as high order accuracy, non-oscillation, conservation and adaptation to the severely distorted fluid problems. The design of the implicit-explicit high order conservative finite difference schemes, the extension of the high order conservative finite difference schemes to three-dimensional 3-T RH equations and the adaptation to multi-material problems constitute our future work.

References

[1] R. Abgrall, P. Bacigaluppi and S. Tokareva, *A high-order nonconservative approach for hyperbolic equations in fluid dynamics*, Computers and Fluids, 169 (2018), 10-22.

[2] S. Atzeni and J. Meyer-ter-Vehn, *The Physics of Inertial Fusion: Beamplasma Interaction, Hydrodynamics, Hot Dense Matter*, Oxford University Press, 2004.

[3] R. Chauvin, S. Guisset and L. Martaud, *A colocalized scheme for three-temperature Grey diffusion radiation hydrodynamics*, Communications in Computational Physics, 31 (2022), 293-330.

[4] J. Cheng and F. Zhang, *A two-dimensional multi-material ALE method for compressible flows using coupled volume of fluid and level set interface reconstruction*, International Journal of Numerical Methods in Fluids, 95 (2023), 1870-1887.

[5] J. Cheng, F. Zhang and T. Liu, *A discontinuous Galerkin method for the simulation of compressible gas-gas and gas-water two-medium flows*, Journal of Computational Physics, 403 (2020), 109059.

[6] J. Cheng, C.-W. Shu and Q. Zeng. *A conservative lagrangian scheme for solving compressible fluid flows with multiple internal energy equations*, Communications in Computational Physics, 12 (2012), 1307-1328.

[7] J. Cheng, N. Lei and C.-W. Shu, *High order conservative Lagrangian scheme for three-temperature radiation hydrodynamics*, Journal of Computational Physics, 496 (2024), 112595.

[8] Y. Cheng and C.-W. Shu, *A discontinuous Galerkin finite element method for directly solving the Hamilton-Jacobi equations*, Journal of Computational Physics, 223 (2007), 398-415.

[9] R.P. Drake, *Radiation Hydrodynamics*, Springer-Verlag: Berlin Heidelberg, 2006.

[10] M. Fatenejad, B. Fryxell, J. Wohlbier, E. Myra, D. Lamb, C. Fryer and C. Graziani, *Collaborative comparison of simulation codes for high-energy-density physics applications*, High Energy Density Physics, 9 (2013), 63-66.

[11] S. Gottlieb, C.-W. Shu and E. Tadmor, *Strong stability-preserving high-order time discretization methods*, SIAM Review, 43 (2001), 89-112.

[12] G.-S. Jiang and C.-W. Shu, *Efficient Implementation of Weighted ENO Schemes*, Journal of Computational Physics, 126 (1996), 202-228.

[13] D. Mihalas and B. W. Mihalas, *Foundations of Radiation Hydrodynamics*, Oxford University Press, 1984.

[14] T. Shiroto, S. Kawai and N. Ohnishi, *Structure-preserving operators for thermal-nonequilibrium hydrodynamics*, Journal of Computational Physics, 364 (2018), 1-17.

[15] C.-W. Shu, *Essentially non-oscillatory and weighted essentially non-oscillatory schemes for hyperbolic conservation laws*, In: Cockburn, B., Johnson, C., Shu, C.-W., Tadmor, E. and Quarteroni, A., Eds, Advanced Numerical Approximation of Nonlinear Hyperbolic Equations Lecture Notes in Mathematics, Springer, Berlin 1697 (1998), 325-432.

[16] C.-W. Shu and S. Osher, *Efficient implementation of essentially non-oscillatory shock-capturing schemes*, Journal of Computational Physics, 77 (1988), 439-471.

[17] C.D. Sijoy and S. Chaturvedi, *TRHD: Three-temperature radiation hydrodynamics code with an implicit non-equilibrium radiation transport using a cell-centered monotonic finite volume scheme on unstructured-grids*, Computer Physics Communications, 190 (2015), 98-119.

[18] C.D. Sijoy and S. Chaturvedi, *Combining node-centered parallel radiation transport and higher-order multi-material cell-centered hydrodynamics methods in three-temperature radiation hydrodynamics code TRHD*, Computer Physics Communications, 203 (2016), 94-109.

[19] Y.-T. Zhang, J. Shi, C.-W. Shu and Y. Zhou, *Numerical viscosity and resolution of high-order weighted essentially nonoscillatory schemes for compressible flows with high Reynolds numbers*, Physical Review E, 68 (2003), 046709.

[20] Y.-T. Zhang, C.-W. Shu and Y. Zhou, *Effects of shock waves on Rayleigh-Taylor instability*, Physics of Plasmas, 13 (2006), 062705.